The importance of cloud properties when assessing surface melting in an offline coupled firn model over Ross Ice shelf, West Antarctica

Nicolaj Hansen[1,2], Andrew Orr[3], Xun Zou[4], Fredrik Boberg[2], Thomas J. Bracegirdle[3], Ella Gilbert[3], Peter L. Langen[5], Matthew A. Lazzara[6,7], Ruth Mottram[2], Tony Phillips[3], Ruth Price[3], Sebastian B. Simonsen[1], and Stuart Webster[8]

[1]Geodesy and Earth Observation, DTU-Space, Technical University of Denmark, Lyngby, Denmark
[2]Danish Meteorological Institute, Copenhagen, Denmark
[3]British Antarctic Survey, High Cross, Madingley Road, Cambridge, UK
[4]Scripps Institute of Oceanography, La Jolla, USA
[5]iClimate, Department of Environmental Science, Aarhus University, Denmark
[6]Madison Area Technical College, Madison, Wisconsin
[7]University of Wisconsin–Madison, Madison, Wisconsin
[8]Met Office, Exeter, United Kingdom

Correspondence: Nicolaj Hansen (nih@dmi.dk)

Abstract. The Ross Ice Shelf, West Antarctica, experienced an extensive melt event in January 2016. We examine the representation of this event by the HIRHAM5 and MetUM high-resolution regional atmospheric models, as well as a sophisticated offline coupled firn model forced with their outputs. The model results are compared with satellite-based estimates of melt days. The firn model estimates of the number of melt days are in good agreement with the observations over the eastern and central sectors of the ice shelf, while the HIRHAM5 and MetUM estimates based on their own surface schemes are considerably underestimated, possibly due to deficiencies in these schemes and an absence of spin-up. However, the firn model simulates sustained melting over the western sector of the ice shelf, in disagreement with the observations that show this region as being melt-free. This is attributed to deficiencies in the HIRHAM5 and MetUM output, and particularly a likely overestimation of nighttime net surface radiative flux. This occurs in response to an increase in nighttime downwelling longwave flux from around 180-200 W m^{-2} to 280 W m^{-2} over the course of a few days, leading to an excessive amount of energy at the surface available for melt. Satellite-based observations show that this change coincides with a transition from clear-sky conditions to clouds containing both liquid-water and ice-water. The models capture the initial clear-sky conditions but seemingly struggle to correctly represent cloud properties associated with the cloudy conditions, which we suggest is responsible for the radiative flux errors.

1 Introduction

Intense and/or prolonged atmospheric-induced melting can result in widespread surface meltwater ponds over Antarctic ice shelves (Kingslake et al., 2017; Stokes et al., 2019). This can lead to the ice shelves thinning and even potentially collapsing if the meltwater enters the ice and results in enough pressure to cause hydrofracturing (Scambos et al., 2000, 2009; Kuipers Munneke et al., 2014), resulting in an increase in the discharge of grounded ice into the ocean and thus higher global sea levels (Dupont and Alley, 2005; Pritchard et al., 2012; Shepherd et al., 2018; Otosaka et al., 2023). Surface melting of ice shelves occurs when the upper surface temperature is greater than the freezing point of ice/snow of 0°C, as well as at sub-freezing temperatures (<0°C) if the snowpack consists of larger snow grains (Nicolas et al., 2017; Jakobs et al., 2021; Orr et al., 2023).

The relatively high temperatures that are associated with Antarctic ice shelf melting are usually in response to local and mesoscale circulations such as barrier winds, katabatic winds, and foehn winds (Orr et al., 2004, 2023; Coggins et al., 2014; Lenaerts et al., 2017a; Heinemann et al., 2019; Zou et al., 2021, 2023; Gilbert et al., 2022), as well as synoptic scale circulation patterns that facilitate the incursion of warm maritime airmasses, such as atmospheric rivers (Nicolas and Bromwich, 2011; Nicolas et al., 2017; Bozkurt et al., 2018; Scott et al., 2019; Wille et al., 2019, 2022; Turner et al., 2022). Therefore, to realistically capture local climate variability and simulate ice shelf melt patterns, it is essential to utilize regional atmospheric models at high spatial resolution, i.e., grid box sizes of the order 10 km or less. High-resolution simulations significantly enhance the description of crucial local-scale atmospheric processes and phenomena, particularly the complex forcing that characterises the Antarctic coastal margins, as well as resolving the smaller ice shelves that exist on spatial scales of 10-100 km (Owinoh et al., 2005; Orr et al., 2005, 2014, 2023; Deb et al., 2018; Lenaerts et al., 2017b).

An additional challenge faced by regional atmospheric models is to realistically represent the surface melting in response to atmospheric-induced warming and the resulting changes to the properties of snow/firn in the upper part of the ice shelf (Firn Symposium team, 2024). This includes aspects such as meltwater production and ponding on the surface, snowmelt-albedo feedback, and retention and refreezing of liquid meltwater in the firn layer (Best et al., 2011; Trusel et al., 2015; Van Wessem et al., 2018; Walters et al., 2019; Jakobs et al., 2021; Keenan et al., 2021). The ability and sophistication of land surface and subsurface snow schemes in regional atmospheric models to represent these effects varies considerably, with the choice of spin-up time for the evolution of the snow/firn layer also being a factor in performance (Van Wessem et al., 2018; Carter et al., 2022). Dedicated and sophisticated offline coupled firn models serve as valuable tools to address these deficiencies (Langen et al., 2017; Keenan et al., 2021).

Cloud properties, particularly cloud phase and microphysics, are typically challenging for regional atmospheric models to represent (Bodas-Salcedo et al., 2012; Abel et al., 2017; Hyder et al., 2018; Gilbert et al., 2020). For example, processes occurring at sub-grid scale, such as vapour deposition and turbulence, can influence the partitioning of available water vapour between the solid and liquid phase, with consequent impacts on the radiative properties of the cloud (Furtado et al., 2016; Kim et al., 2020; Kretzschmar et al., 2020). Poor representation of these processes by the single-moment cloud microphysics scheme used by the UK Met Office Unified Model (MetUM) has led to clouds containing too much ice water content and not

enough liquid water content (Abel et al., 2017), leading to considerable biases in surface energy balance (SEB) as clouds with larger quantities of liquid water (relative to ice) are associated with higher downwelling longwave (LW) fluxes reaching the surface, while clouds containing more ice (relative to liquid) are associated with higher downwelling shortwave (SW) fluxes reaching the surface (Zhang et al., 1996). Such biases in SEB are therefore also associated with errors in surface melting in Antarctica (King et al., 2015; Gilbert et al., 2020). Properties such as cloud height, temperature and droplet/crystal size can also impact the radiative effect of the cloud, often in complex and contrasting ways (Lawson and Gettelman, 2014; Barrett et al., 2017; Gilbert et al., 2020). Errors with respect to the vertical distribution of liquid and ice, and especially the representation of thin supercooled liquid layers within mixed-phase clouds, can induce radiative biases (Gilbert et al., 2020; Vignon et al., 2021; Inoue et al., 2021). In addition to microphysics, model cloud macrophysical parameterisations, especially relating to cloud fraction (horizontal and vertical), may impact cloud radiative effects (Van Weverberg et al., 2023; McCusker et al., 2023).

Here we investigate the benefits of applying the sophisticated offline coupled firn model described by Langen et al. (2017) that represents key aspects such as the melt-albedo feedback to improve regional atmospheric model simulations of a prolonged and extensive episode of surface melt that occurred during January 2016 over the Ross Ice Shelf (RIS), West Antarctica. The RIS frequently experiences major surface melt events due to both synoptic- and local-scale processes (Nicolas et al., 2017; Zou et al., 2021; Li et al., 2023; Orr et al., 2023), with this particular event attributed to an influx of warm and moist marine air, likely linked to a concurrent strong El Niño episode (Nicolas et al., 2017).

Assessing the ability of models to estimate surface melt on Antarctic ice shelves is important for identifying deficiencies and aspects of the models that will require improvements in the future. Studies show that summertime surface melting of Antarctic ice shelves will likely increase considerably in the future (Trusel et al., 2015; Kittel et al., 2021; Feron et al., 2021; Gilbert and Kittel, 2021; Boberg et al., 2022; van Wessem et al., 2023). For example, Trusel et al. (2015) suggests that scenario-independent doubling of Antarctic-wide melt will occur by 2050, and also that surface melt on several ice shelves under the high-emission climate scenario will approach the levels that contributed to the recent collapse of Larsen A and B ice shelves on the northern Antarctic Peninsula by 2100. Thus, improving the information on surface melting (and surface mass balance) and using this as an indicator for possible ice shelf collapse (Kuipers Munneke et al., 2014) or accelerations of outlet glaciers (Tuckett et al., 2019) is vital for generating more accurate projections of future Antarctic ice sheet stability and its contribution to sea level rise (Fox-Kemper et al., 2021).

2 Methods and materials

2.1 Models

The regional atmospheric model simulations examined were initially produced for Antarctic CORDEX (Antarctic COordinated Regional Downscaling EXperiment), and are based on HIRHAM version 5 (HIRHAM5) and MetUM version 11.1 (Orr et al., 2023). The HIRHAM5 model combines the physics of the ECHAM5 general circulation model and the hydrostatic dynamical core of the HIRLAM7 numerical weather prediction model (Christensen et al., 2007). The model uses a single-moment microphysics scheme described by Sundqvist (1978). Furthermore, HIRHAM5 incorporates a five-layer snow scheme (extending to

a depth of 10 m water equivalent) described by Langen et al. (2015), which calculates surface melt and the associated retention and refreezing of liquid water in the firn layer. The scheme also represents the dependence of snow albedo on temperature by linearly varying the albedo between 0.85 (for fresh dry snow/temperatures below -5°C) and 0.65 (for wet snow/temperatures at 0°C). The MetUM version 11.1 model uses the Global Atmosphere 6.0 configuration (Walters et al., 2017, GA6), designed for grid scales of 10 km or coarser. This includes the ENDGame (Even Newer Dynamics for General atmospheric modelling of the environment) dynamical core, which solves equations for a non-hydrostatic, fully compressible, deep atmosphere. The model uses a single-moment cloud microphysics scheme based on Wilson and Ballard (1999). For simulating the thermal storage of snow it utilises a "zero-layer" snow scheme described by Best et al. (2011), which employs a composite snow/soil layer and does not account for firn processes.

The physically-based multi-layer offline coupled firn model (hereafter referred to as the firn model) is based on the version implemented in HIRHAM5 (Langen et al., 2015), but heavily updated by Langen et al. (2017) to include 32 vertical layers (extending to a depth of 60 m water equivalent) and a sophisticated firn scheme. The model includes processes such as densification, snow grain growth, irreducible water saturation, impermeable ice layers, and snow state-dependent hydraulic conductivity. This enables a much more detailed representation of retention and refreezing of liquid water within the firn, and thus an improved representation of vertical water flow and refreezing. The version used here is identical to that previously applied to Antarctica by Hansen et al. (2021), which was based on the version optimised for Greenland (Langen et al., 2017; Mottram et al., 2017).

The HIRHAM5 and MetUM simulations were run over the standard Antarctic CORDEX domain (see Fig. 1) at a grid spacing of 0.11°(equivalent to 12 km) from 1979 to 2019, although in this study only output for January 2016 is examined. Lateral- and surface-boundary conditions for both simulations were provided by ERA-Interim reanalysis data (Dee et al., 2011). The HIRHAM5 simulation employed 31 vertical levels in the atmosphere (up to a height of 12.5 hPa), while the MetUM employed 70 vertical levels (up to a height of 80 km). Additionally, while the HIRHAM5 simulation uses a long-term continuous integration approach, the MetUM simulation uses a frequent re-initialisation approach (Lo et al., 2008). This consists of a series of twice-daily 24-hour forecasts (at 00 and 12 UTC), with output at T+12, T+15, T+18, and T+21 hrs from each of the forecasts concatenated together to form a seamless series of 3-hourly model outputs, with the output before T+12 hrs discarded as spin-up. The five-layer snow scheme used by HIRHAM5 was simply initialised and not spun-up. The zero-layer snow scheme used by the MetUM cannot be spun-up as it does not account for firn processes (Best et al., 2011). In any case, the frequent re-initialisation approach used to produce the MetUM simulations would prevent the evolution of any internal snow/firn conditions. The setup for both models is identical to that described in Orr et al. (2023).

The firn model is subsequently driven by atmospheric forcing from the HIRHAM5 and MetUM simulations for the January 2016 period. This consists of 6-hourly averaged values of solid precipitation, liquid precipitation, surface evaporation, surface sublimation, surface downwelling SW radiative flux, surface downwelling LW radiative flux, sensible heat flux, and latent heat flux, which the firn model subsequently interpolates to hourly values before using them as forcing, by performing a linear interpolation in time between the two nearest 6-hourly files. Prior to the simulations of the January 2016 period the firn model is spun-up for a period of 250 years using HIRHAM5 forcing (by repeating the same 1980s decade 25 times) to ensure a more

realistic representation of the snow and firn properties. Following this, the firn model forced with MetUM output is spun-up for an additional 150 years using MetUM output (by repeating the same 1980s decade 15 times), to ensure that the firn pack has a memory of MetUM forcing.

The native surface melt output from the HIRHAM5 and MetUM simulations, as well as output from the HIRHAM5 and MetUM-forced firn model simulations, are used to calculate patterns of daily melt extent (during the January 2016 event. Here, melt days are defined as days with at least 3 mm (water equivalent) of melt occurring (Donat-Magnin et al., 2020))during the January 2016 event. Note that we found that the modelled patterns of daily melt extent were broadly similar for melt thresholds of 1, 3, and 5 mm per day (not shown), but selected 3 mm per day as this is the same threshold used by Lenaerts et al. (2017b); Deb et al. (2018); Donat-Magnin et al. (2020). For all snow/firn models, the energy flux used to melt the surface is calculated as the residual in the SEB whenever the surface temperature reaches above 0°C, after which it is reset to 0°C (Best et al., 2011; Langen et al., 2015, 2017).

2.2 Observations

The modelled patterns of daily melt extent are compared with daily melt extent estimates derived from satellite passive microwave observations of brightness temperature (Picard et al., 2007; Nicolas et al., 2017), which use the same melt threshold of 3 mm and have a grid spacing . Microwave remote sensing is particularly suited to detecting surface meltwater over ice shelves because (a) the appearance of liquid water causes an abrupt increase in brightness temperatures and (b) the observations can be acquired during day and nighttime and clear and cloudy conditions (Picard et al., 2007; Nicolas et al., 2017; Johnson et al., 2020, 2022; Mo . Here, we use a gridded daily surface melting dataset based on Special Sensor Microwave Imager Sounder (SSMIS) satellite-based observations, which uses horizontally polarized brightness temperatures at 19 GHz to identify surface melt. See Nicolas et al. (2017) for further details on the melt detection method. This dataset is available at a spatial resolution of 25 km× 25 km, with each grid point classified as either 1 (meaning melt was detected during the corresponding day) or 0 (melt not detected). We also use measurements of near-surface air temperatures from four automatic weather stations (AWS) situated on the western sector of the RIS (Lazzara et al., 2012) to further determine the occurrence of melt and assess the HIRHAM5 and MetUM models. These stations are referred to as Sabrina, Elaine, Schwerdtfeger, and Marilyn (see Fig. 1 for their locations). A temperature threshold of -2°C is chosen for melting to occur, which is suggested by Nicolas et al. (2017).

Satellite data are used to understand the characteristics and properties of clouds during the melt event, and whether they were important, and how well they were represented by the HIRHAM5 and MetUM models. We use low-level cloud cover from Moderate Resolution Imaging Spectroradiometer (MODIS) satellite-based imagery at a grid spacing of 10 km (Platnick et al., 2015), which agrees broadly with the grid spacing of the HIRHAM5 and MetUM models. However, as no direct observations were available at 12 UTC (over the western region of the RIS), a pseudo-image for this time was calculated by averaging two MODIS images that corresponded to satellite ground tracks passing over the western sector of the RIS at around 06 UTC (from the Aqua satellite) and 18 UTC (from the Terra satellite). To examine the phase of clouds during the event, along-track vertical profiles of ice/liquid clouds are obtained from two orbits of the satellite-based Cloud-Aerosol Lidar and Infrared Pathfinder Satellite Observation (CALIPSO) mission on the 14th and 17th of January (see Fig. 1 for ground tracks). These observations

distinguish between ice (depolarising) and water clouds (spherical) based on backscattered light (Hu et al., 2009). Finally, we also use cloud liquid/ice water paths from Clouds and the Earth's Radiant Energy System (CERES) satellite-based observations (Wielicki et al., 1996; Loeb et al., 2018), which have a grid spacing of $1°$. We use the CERES SYN1deg 3-hourly dataset edition 4.1, which consists of data from multiple geostationary and polar orbiting satellites (CERES, 2017).

Unfortunately the RIS lacks ground observations to offer additional information on the SEB for January 2016, and although the Atmospheric Radiation Measurement (ARM) West Antarctic Radiation Experiment (AWARE) provides valuable SW/LW data at a station on the West Antarctic Ice Sheet, this is too distant from our area of interest to be useful. Additionally, CERES surface fluxes are not utilized in this study due to uncertainties arising from the degradation of Terra water vapor channels after 2008 and potential inaccuracies when clear sky fluxes are employed in the calculation (CERES, 2017). Moreover, Hinkelman and Marchand (2020) suggested a potential positive bias in SW radiation and a negative bias in LW radiation over the Southern Ocean.
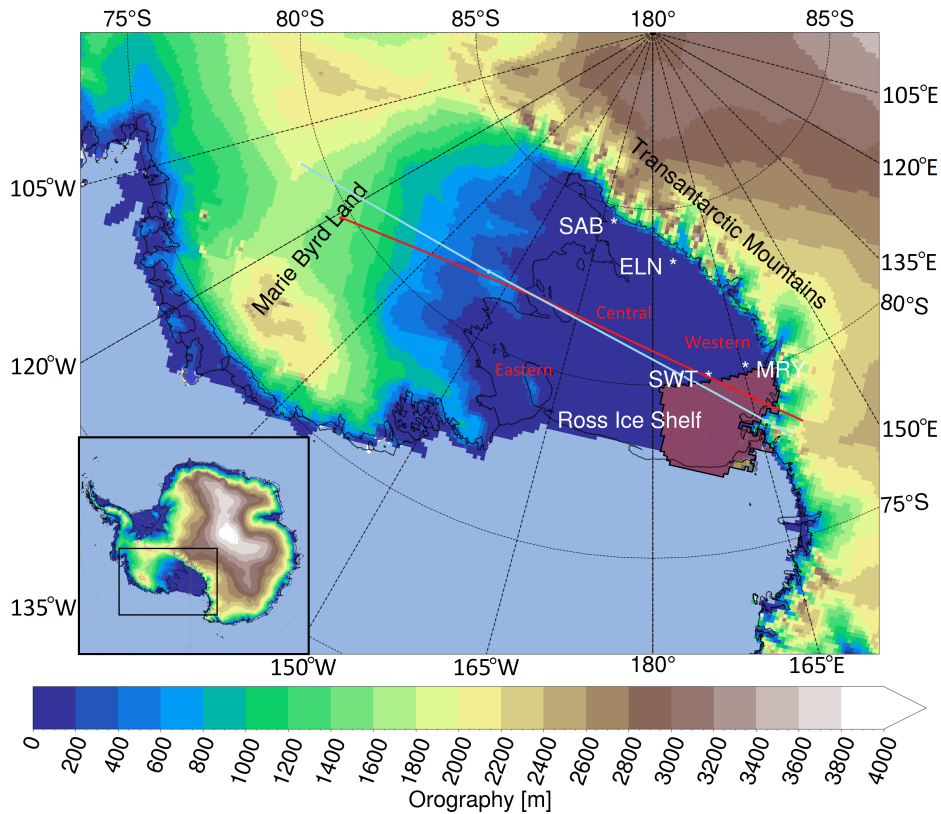
Figure 1. Map of West Antarctica showing the location of the Ross Ice Shelf, Marie Byrd Land, and the Transantarctic Mountains. Also labelled are the eastern, central, and western sectors of the ice shelf, with the eastern sector bordered by Marie Byrd Land and over the left-hand side of the ice shelf on the map, while the western sector is bordered by the Transantarctic Mountains and is over the right-hand side of the map. The orography (shading) and coastline (solid black line) are from the HIRHAM5 model. Also shown are the locations of Sabrina, Elaine, Schwerdtfeger, and Marilyn AWS (labelled SAB, ELN, SWT, and MRY, respectively), which are situated on the western sector of the ice shelf. The area over the western sector of the ice shelf that is investigated in depth is highlighted by the burgundy shading. The two solid lines crossing the ice shelf show the ground tracks of the CALIPSO satellite on the 14th (turquoise) and the 17th (red) of January 2016. The inset map shows the full model domain used for the HIRHAM5 and MetUM simulations.

3 Surface melting

Figure 2 shows that extensive surface melting occurred over much of the central and eastern sectors of the RIS during January 2016, with the total number of satellite-observed melt days for this period approaching up to 15 in these locations. Examination of the observed melt pattern for individual days showed this period occurred roughly from the 11th to 25th of January (not shown). Much fewer melt days are observed over the western sector of the RIS during this period, with the transition between the high melt regime to the east and the low melt regime to the west abruptly occurring around 180°W, as also shown by Nicolas et al. (2017). Figure 2 also shows a considerable underestimation in the total number of melt days calculated from the

native melt output from HIRHAM5 and MetUM. This is especially apparent for HIRHAM5, which simulates only a few melt days over the eastern sector of the RIS and no melt days over the central sector. The MetUM performance is slightly better in terms of both the number (up to 10) and pattern of the melt days, with the latter broadly agreeing with the observations. However, there is a considerable increase in the number of melt days calculated from melt output from the firn model forced by HIRHAM5 and MetUM, with up to 20 melt days simulated over the entire RIS. Although the firn model results are in better agreement with the observations over the eastern and central sectors of the RIS (albeit they now slightly overestimate the number of melt days in these areas), they erroneously simulate a much higher number of melt days (up to 20) over the western sector of the RIS compared to the satellite-based observations.

To investigate further the discrepancies between the number of melt days estimated from the firn model and the observations, Fig. 3 compares model and satellite-based maps of daily melt area from the 13th to 18th of January. These six days were selected out of all of January because they (a) coincided with the main period of surface melting that occurred, and (b) showed the largest differences between the observations and firn model results, especially over the western RIS sector. The satellite-based observations show a distinct melt-free region over the western sector of the RIS on each of these six days compared to the central and eastern sectors that show melt (i.e., broadly consistent with the observed surface melt pattern shown in Fig. 2a for all of January). This pattern is largely well simulated by the firn model from the 13th to 15th of January. However, from the 16th to 18th of January, the firn model results erroneously show a much smaller melt-free region over the western sector of the RIS compared to the observations, which gets progressively smaller each day. By the 17th and 18th of January any melt-free area over the RIS is non-existent in the HIRHAM5-forced results and limited to the extreme western margins of the RIS in the MetUM-forced results.

The AWS-measured near-surface air temperatures from the 13th to 18th of January (Fig. 4) are consistent with the satellite-based melt patterns (Fig. 3). For example, Sabrina AWS and Elaine AWS both show temperatures above the -2°C threshold for melt during this period, consistent with both sites being located in a region where the satellite-based measurements show melting. By contrast, Schwerdtfeger AWS and Marilyn AWS show temperatures that are either around or below this threshold, consistent with both sites being located in the western sector of the RIS that the satellite-based measurements identify as being melt-free during this period. Moreover, the erroneous regions of melt over the western RIS simulated by the firn model during this period are consistent with near-surface air temperatures simulated by HIRHAM5 and MetUM being higher than the AWS-measured temperatures in this region, and especially at Schwerdtfeger and Marilyn temperatures observed by Schwerdtfeger AWS and Marilyn AWS (Fig. 4). In particular, at these two stations the HIRHAM5 near-surface temperatures are consistently above -2°C from the 16th to 18th, while the measurements are below this threshold. This is the threshold for melting for this particular event suggested by Nicolas et al. (2017).
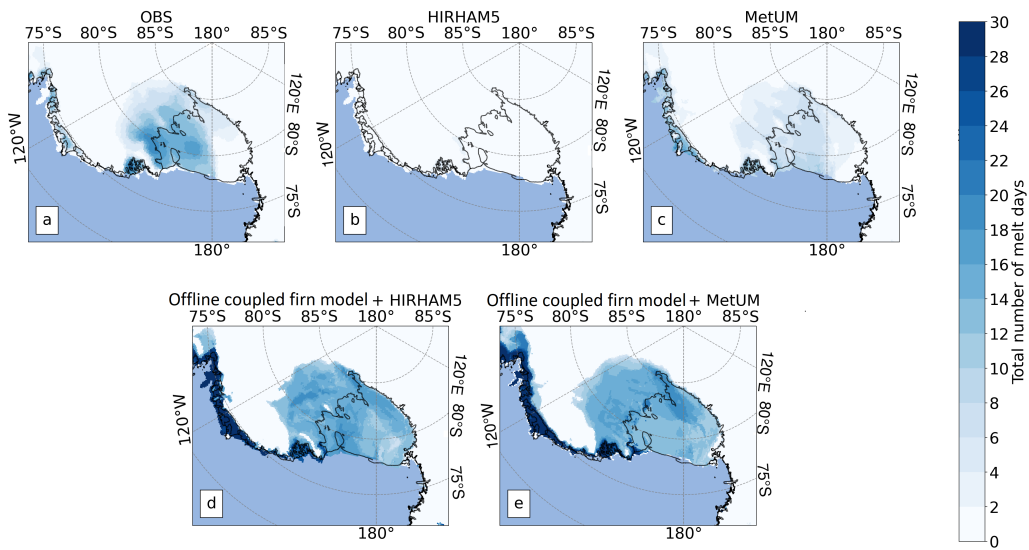
Figure 2. Maps of West Antarctica showing the total number of melt days (shading) during January 2016 from (a) satellite passive microwave measurements, (b) native melt output from HIRHAM5, (c) native melt output from MetUM, (d) melt output from the offline coupled firn model forced by HIRHAM5 output, and (e) melt output from the offline coupled firn model forced by MetUM output.
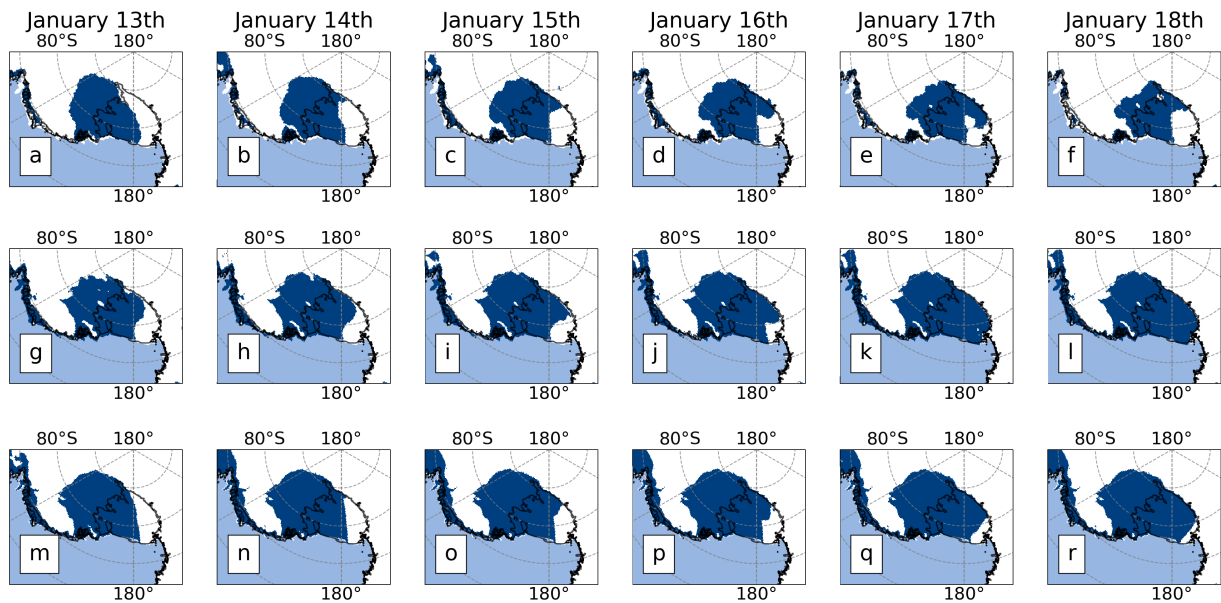
Figure 3. Maps of West Antarctica showing the daily melt area from the 13th to 18th (from left to right) of January 2016 from (top row; a-f) satellite passive microwave measurements, (middle row; g-l) the offline coupled firn model forced by HIRHAM5 output, and (bottom row; m-r) the offline coupled firn model forced by MetUM output. Melt areas are indicated by the dark shading, while melt-free regions are shown as white.
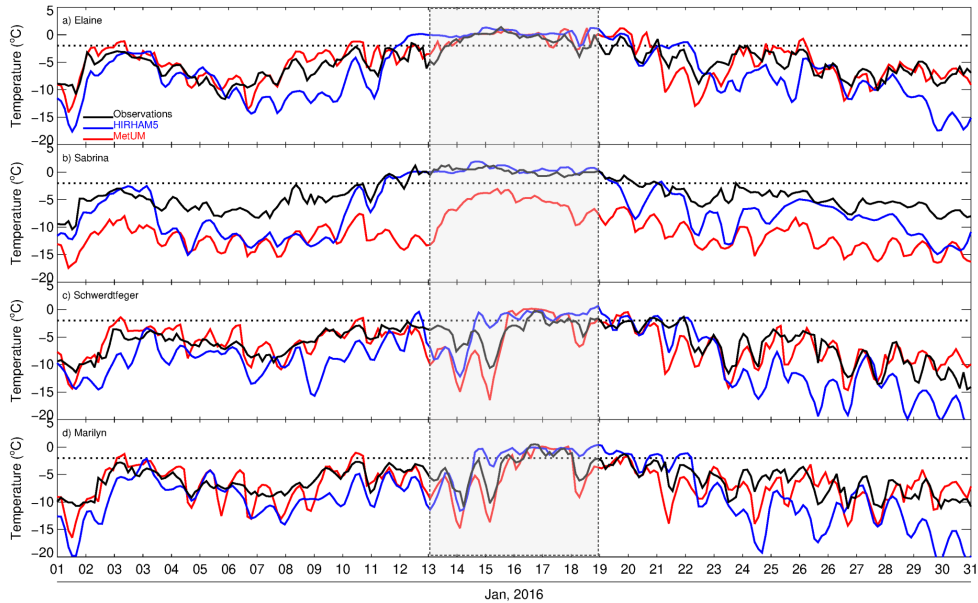
Figure 4. Timeseries of near-surface air temperature (°C) from the 1st to 31st of January 2016 from AWS measurements (black line), HIRHAM5 output (blue line), and MetUM output (red line) at (a) Elaine, (b) Sabrina, (c) Schwerdtfeger, and (d) Marilyn. The period of special interest from 13th to 18th of January is highlighted by the semi-transparent shaded region. The date shown is in UTC, with local time for the Ross Ice Shelf 12 hrs ahead of UTC. The horizontal dotted line shows temperatures at -2°C, which Nicolas et al. (2017) suggests is the threshold for melting for this particular event.

4   Surface radiative fluxes

The firn model simulation of daily melt extent over the western sector of the RIS is broadly in agreement with the satellite-based observations from the 13th to 15th and then in disagreement from the 16th to 18th (Fig. 3). To investigate this, Fig. 5 compares the timeseries for this period of surface radiative fluxes that are spatially-averaged over the western sector of the RIS (region highlighted in Fig. 1) from HIRHAM5 and MetUM. For the initial part of the timeseries from the 13th to 14th, the diurnal cycle of net surface radiative flux shows negative values during nighttime of around -20 to -40 W m^{-2} for HIRHAM5 and around -20 W m^{-2} for MetUM, which are broadly consistent with freezing and thus with the firn models correctly simulating this region as being melt-free. Note that the models also show positive net surface radiation values during daytime, suggesting a daily freeze-thaw cycle. However, from the 15th to 18th the models simulate a transition towards values of nighttime/minimum net surface radiation flux of around zero, which is broadly consistent with an absence of freezing and the firn models (erroneously) simulating surface melt. It is also apparent that although the minimum net surface radiation is broadly similar for both models,

the daytime maximum net surface radiation values are larger for HIRHAM5 compared to MetUM, e.g., for the 16th, 17th, and 18th the HIRHAM5 values are around 50, 10 and 20 W m^{-2} larger than those of MetUM. This is possibly consistent with the HIRHAM5-forced firn model estimate of melt extent being much more (erroneously) extensive over the western RIS compared to the MetUM-forced estimate (Fig. 3), as well as HIRHAM5 simulating warmer near-surface temperatures over this region compared to MetUM (Fig. 4). Note that the diurnal cycle of SEB from the models broadly follows the net surface radiative flux cycle. For example, the nighttime/minimum SEB values from the models shows negative values for the initial part of the timeseries and zero/positive values for the later part of the timeseries. This suggests that the primary energy source responsible for the transition in SEB is from surface radiative flux and not sensible and latent heat fluxes (Nicolas et al., 2017).

Examination of the timeseries of net surface SW and net surface LW fluxes from HIRHAM5 and MetUM in Fig. 5 suggests that the radiative fluxes are finely balanced with respect to surface melt. In particular, the transition from negative values of nighttime/minimum net surface radiation flux to zero/positive values is mainly due to net surface LW values becoming less negative. For example, values of net surface LW flux change from -90 to -100 W m^{-2} on the 14th and 15th to around -20 W m^{-2} on the 17th and 18th. By contrast, the net surface SW values show little change in either direction at night (as expected), i.e., they are unable to offset the changes in net surface LW flux. Figure 5 further shows that the changes in net surface LW values are due to a marked increase in surface downwelling LW flux, which increases from around 180 to 200 W m^{-2} on the 14th and 15th to around 280 W m^{-2} on the 17th and 18th.

To further understand the discrepancies in melt area over the western RIS region, Figs. 6, 7, and 8 show the spatial distributions of net surface radiative flux, net surface LW flux, and surface downwelling LW flux, respectively, from HIRHAM5 and MetUM, at 12 UTC on the 14th of January and 12 UTC on the 17th of January, i.e., representative of nighttime conditions as the local time for the Ross Ice Shelf is 12 hrs ahead of UTC. Figure 6 shows that the negative net surface radiative flux values simulated by HIRHAM5 and MetUM over the western RIS during nighttime on the 14th are actually largely constrained to this region and do not extend over the rest of the RIS. Over this region the values are around -35 W m^{-2} for HIRHAM5 and slightly smaller for MetUM (c.f., Fig. 5). By contrast, over the central and eastern sectors of the RIS the simulated values of net surface radiative flux are mostly positive, i.e., consistent with the firn model simulating melting here, in agreement with the observations. Figure 6 also shows that the region of weakly positive net surface radiative values (around zero) simulated by the models during nighttime on the 17th (c.f., Fig. 5) actually extends over the entire western sector of the RIS, i.e., the sector bordering the entire length of the Transantarctic Mountains. By contrast, the simulated net surface radiative values over the eastern and central sectors of the ice shelf are largely negative during nighttime on the 17th.

Figure 7 shows that the large negative net surface LW fluxes of up to -100 W m^{-2} simulated by HIRHAM5 and MetUM over the western sector of the RIS during nighttime on the 14th are also largely constrained to this region (c.f. Fig. 5), with the negative values over the central and eastern sectors of the ice shelf considerably smaller compared to the western region. The results also confirm the transition to much smaller negative values of net surface LW fluxes during nighttime from the 14th to the 17th over this region (c.f. Fig. 5). However, over the central and eastern sectors of the RIS during nighttime on the 17th the simulated negative net surface LW fluxes are markedly larger than the values over the western sector.

245   The marked increase in surface downwelling LW flux simulated by the models over the western sector of the RIS during nighttime is confirmed in Fig. 8, with values around 200 W m^{-2} on the 14th and around 280 W m^{-2} on the 17th (c.f. Fig. 5). Also apparent is that the surface downwelling LW flux over the central and eastern sectors of the RIS during nighttime on the 14th is considerably larger compared to the western sector, which is consistent with Fig. 7. Note that examination of the net surface SW flux simulated by the models showed broadly similar values on the 14th and the 17th over the western RIS during nighttime
250   (not shown).
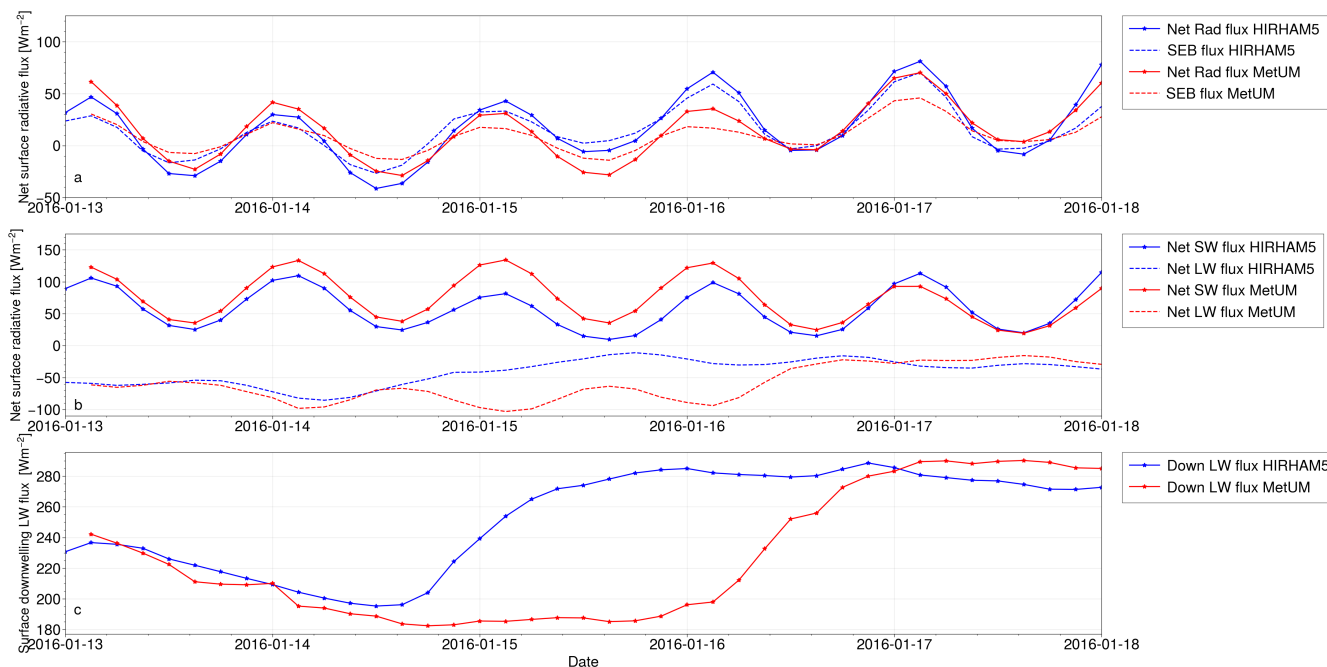
Figure 5. Timeseries of surface radiative fluxes from the 13th to 18th of January 2016 that are spatially-averaged over the western sector of the RIS (region highlighted in Fig. 1) from HIRHAM5 and MetUM simulations (W m^{-2}). Panel (a) shows the net surface radiative fluxes and SEB. Panel (b) shows the net surface LW and SW fluxes. Panel (c) shows the surface downwelling LW fluxes. The date shown is in UTC, with local time for the Ross Ice Shelf 12 hrs ahead of UTC.
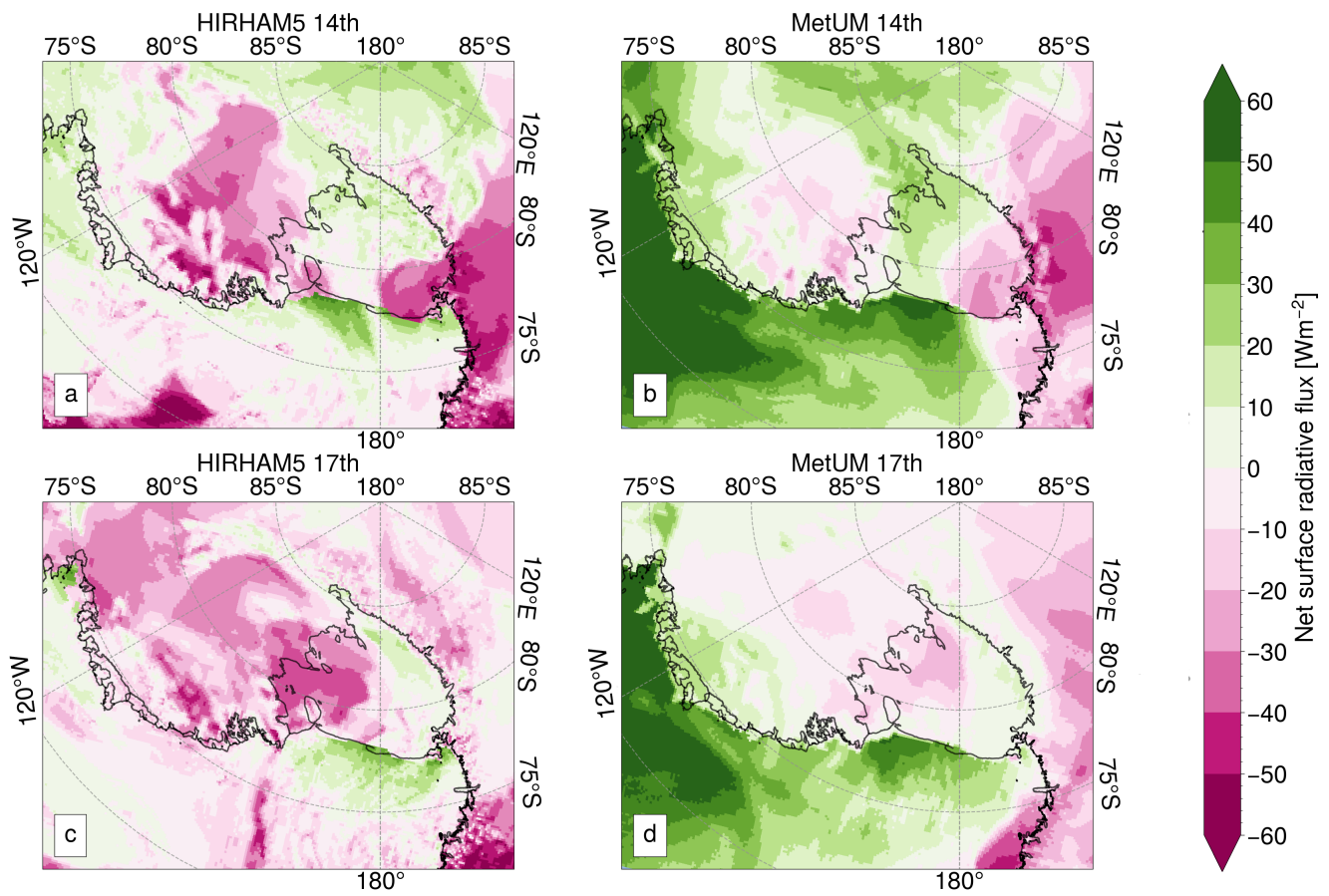
Figure 6. Maps of West Antarctica showing 3-hourly averaged net surface radiative fluxes (W m^{-2}) at 12 UTC on the 14th of January 2016 (top row; a, b) and 12 UTC on the 17th of January 2016 (bottom row; c, d) from HIRHAM5 (left column; a, c), MetUM (right column; b, d). Downward fluxes are positive. Note that 12 UTC is equivalent to 00 LT over the Ross Ice Shelf.
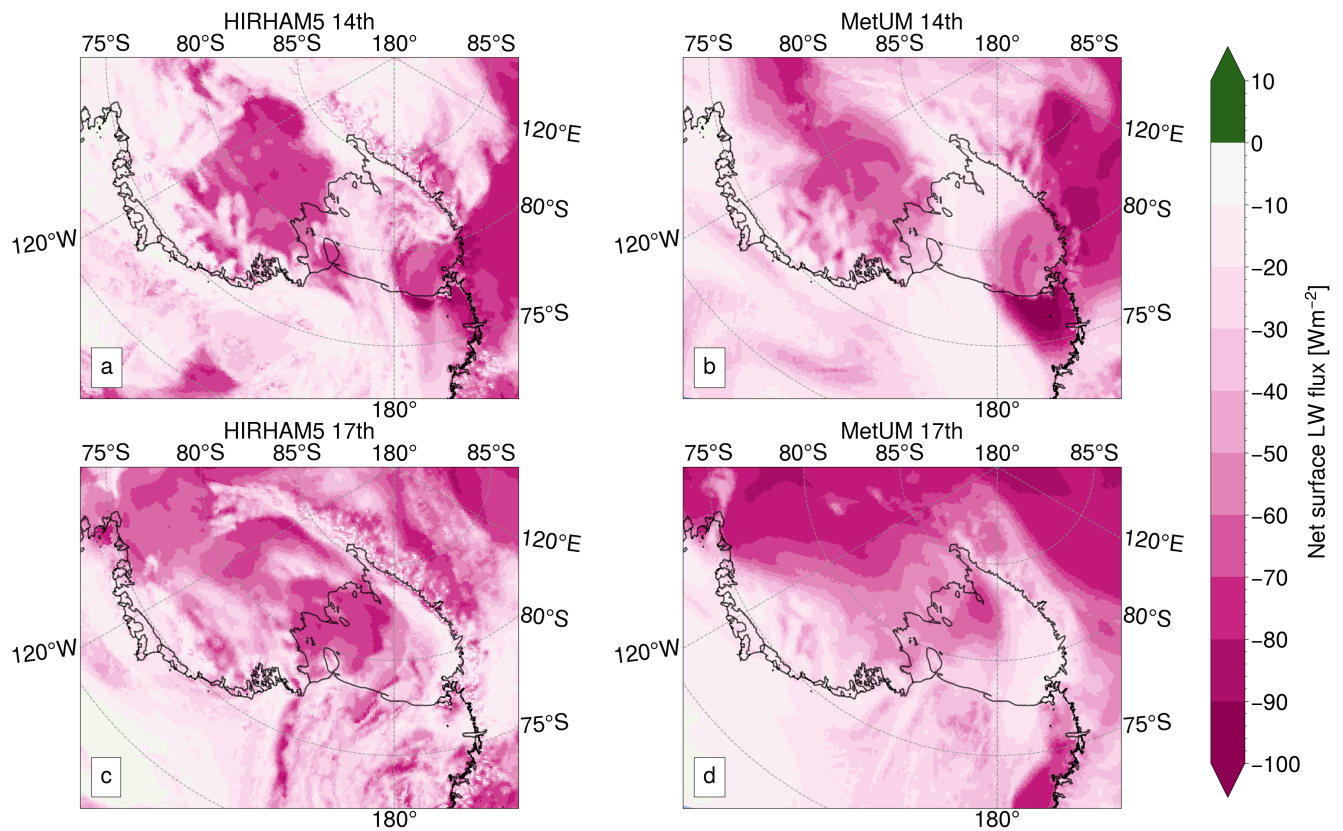
Figure 7. Maps of West Antarctica showing 3-hourly averaged net surface LW fluxes (W m^{-2}) at 12 UTC on the 14th of January 2016 (top row; a, b) and 12 UTC on the 17th of January 2016 (bottom row; c, d) from HIRHAM5 (left column; a, c), MetUM (right column; b, d). Downward fluxes are positive. Note that 12 UTC is equivalent to 00 LT over the Ross Ice Shelf.
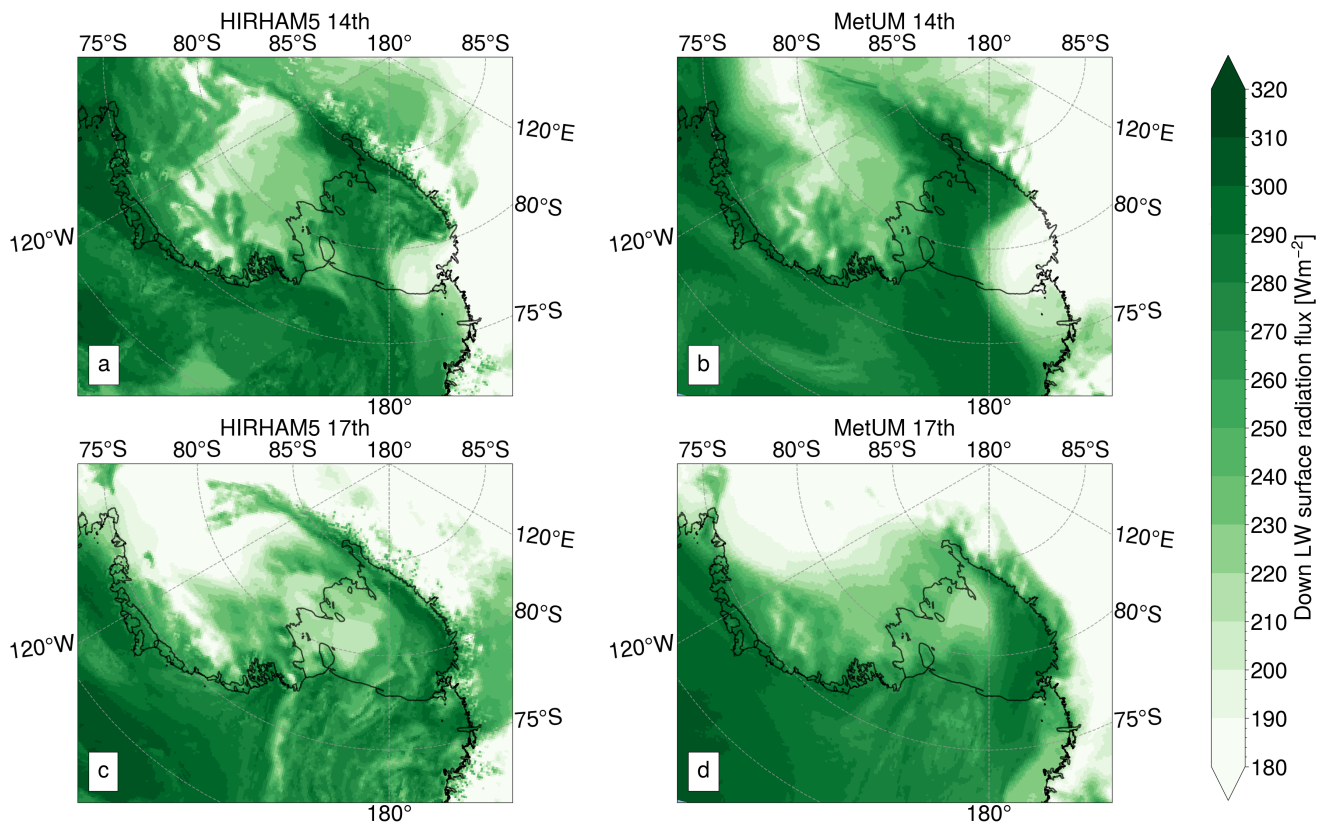
Figure 8. Maps of West Antarctica showing 3-hourly averaged surface downwelling LW fluxes (W m^{-2}) at 12 UTC on the 14th of January 2016 (top row; a, b) and 12 UTC on the 17th of January 2016 (bottom row; c, d) from HIRHAM5 (left column; a, c), MetUM (right column; b, d). Downward fluxes are positive. Note that 12 UTC is equivalent to 00 LT over the Ross Ice Shelf.

5   Cloud properties

Figures 9 to 12 compare cloud properties between the 14th and the 17th of January to help explain the differences in radiative fluxes (Figs. 5 to 8) over the western sector of the RIS. Figure 9 shows the low-level cloud fraction from HIRHAM5 and the MetUM at 12 UTC on the 14th January and 12 UTC on the 17th January, i.e., the same times as examined in Figs. 6 to 8. Also

255   shown are MODIS observations at these times. On the 14th of January, the models show largely cloud-free conditions over the western RIS region (0%), in contrast to extensive cloud over the melting-areas of the eastern and central sectors of the RIS (>80%). However, on the 17th of January the simulations show extensive cloud cover over the western and central sectors of the RIS and more cloud-free conditions over the eastern sector. Note that the HIRHAM5 and MetUM simulated medium- and upper-level cloud fractions showed cloud-free conditions during these times (not shown). The model estimates of cloud cover

260   on both the 14th and 17th are largely in agreement with the MODIS imagery, especially over the western RIS region - although MODIS shows a slightly smaller cloud-free area over this region on the 14th compared to the models.

The good agreement between simulated and observed cloud cover over the western RIS (Fig. 9) suggests that the errors in surface melting which we attribute to the potential misrepresentation of net surface LW and surface downwelling LW fluxes may stem from factors beyond simple cloud cover to other processes such as cloud microphysics. This is examined by Fig. 10,

265 which shows the vertical profile of cloud phases and their respective heights retrieved by CALIPSO during its passage over the western RIS at around 06 UTC on 14th and 17th January – note that the difference in times compared to Fig. 9 makes a direct comparison difficult. Nevertheless, CALIPSO detected mostly liquid-based clouds between 2-4 km above the RIS on 14th of January, including this western sector (Fig. 10). Although it is ~~noteworthy that the satellite track over this region was relatively far north, and at 06 UTC~~ worth pointing out that over the western sector of the RIS on 14th of January that the MODIS imagery

270 ~~showed cloudy conditions over the north-western sector of RIS~~ shows cloudy conditions at 06 UTC (not shown) ~~. However, as mentioned above, MODIS imagery confirms that the western sector of the RIS can be considered as~~ and largely cloud-free ~~on the 14th~~ conditions at 12 UTC (Fig. 9). More noteworthy is that CALIPSO shows ~~mixed-phase~~ liquid-water and ice-water clouds extending up to 7 km above the surface ~~in the same region on the 17th~~ of the western sector of the RIS on the 17th of January (Fig. 10)~~coincident with~~, i.e., over the same region that the models show the (erroneous) spike in ~~modelled melt.~~

275 melt. Additionally, the occurrence of liquid-based clouds on the 14th and 17th of January in the CALIPSO observations over the eastern and central sectors of the RIS is consistent with the satellite-based measurements showing melting here (Fig. 3).

As shown by Fig. 11, the MetUM simulates negligible values of cloud liquid and ice water content over the western sector of the RIS on the 14th of January at 12 UTC, consistent with the cloud-free conditions also simulated over this area at this time (Fig. 9). Figure 12 shows equivalent results for CERES, which also indicates negligible values of cloud ice/liquid water path

280 at 12 UTC on the 14th of January over the western sector of the RIS. On the 17th ~~January~~ of January at 12 UTC the MetUM simulates much higher amounts of cloud ice-water over the western sector of the RIS compared to cloud liquid-water, with a maximum cloud ice water path of around 0.5 kg m^{-2}. However, CERES suggests that clouds with high ice *and* liquid water content occur at 12 UTC on the 17th over this region, with a cloud ice water path comparable to the MetUM (up to 0.5 kg m^{-2}) but with cloud liquid water path up to 1 kg m^{-2}; two orders of magnitude larger than that simulated by the MetUM. During this

285 time, CALIPSO also observed liquid-water and ice-water clouds over the western region of the RIS (Fig. 10), which supports the CERES results.
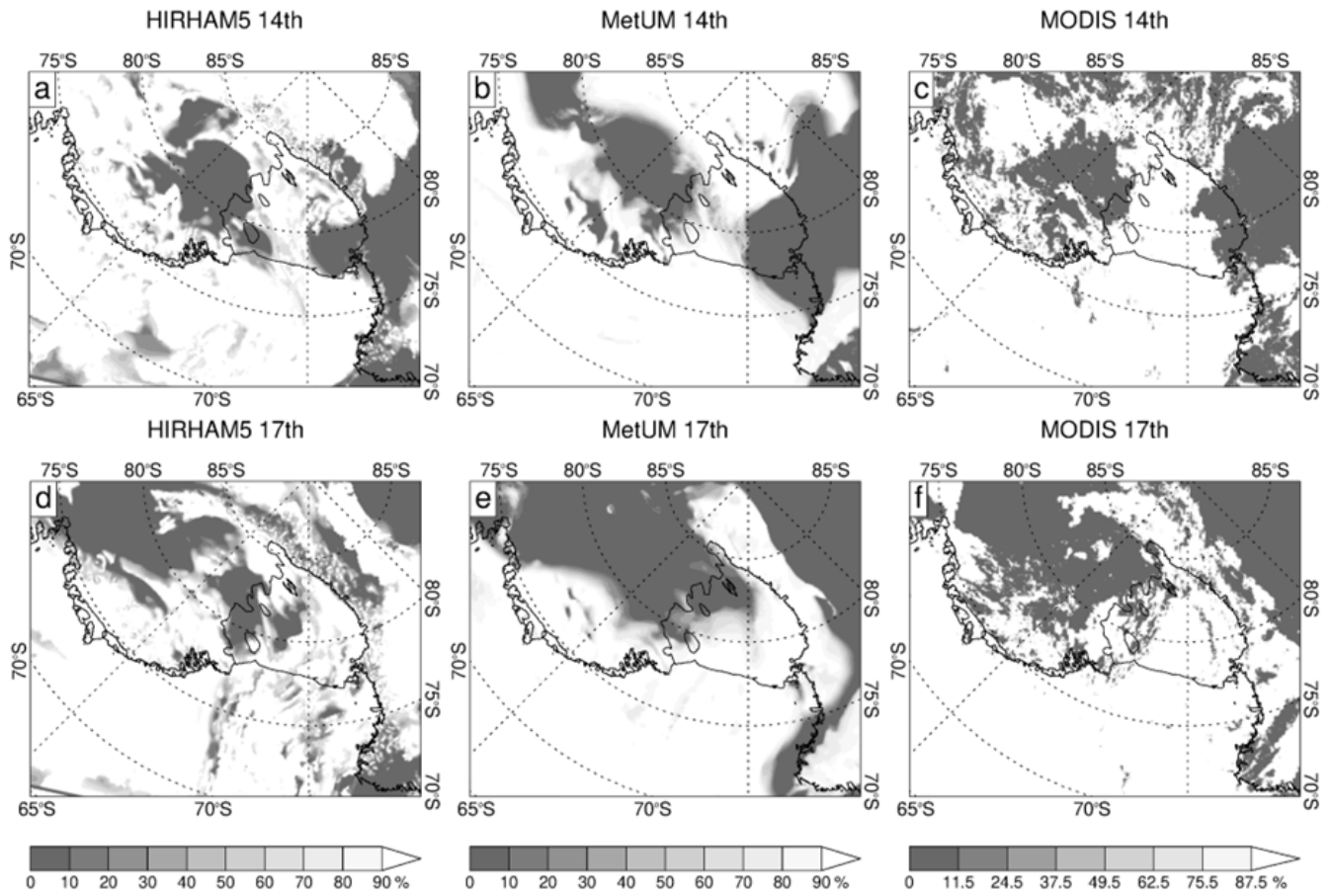
Figure 9. Maps of West Antarctica showing cloud cover (%) at 12 UTC on the 14th of January 2016 (top row; a-c) and 12 UTC on the 17th of January 2016 (bottom row; d-f) from HIRHAM5 (left column; a, d), MetUM (middle column; b, e), and MODIS (right column; c, f). The model results are based on 6-hourly averages of low-level cloud fraction. For MODIS, a pseudo-image at 12 UTC was calculated by averaging two MODIS images that corresponded to satellite ground tracks over the western sector of the RIS at around 06 UTC and 18 UTC.
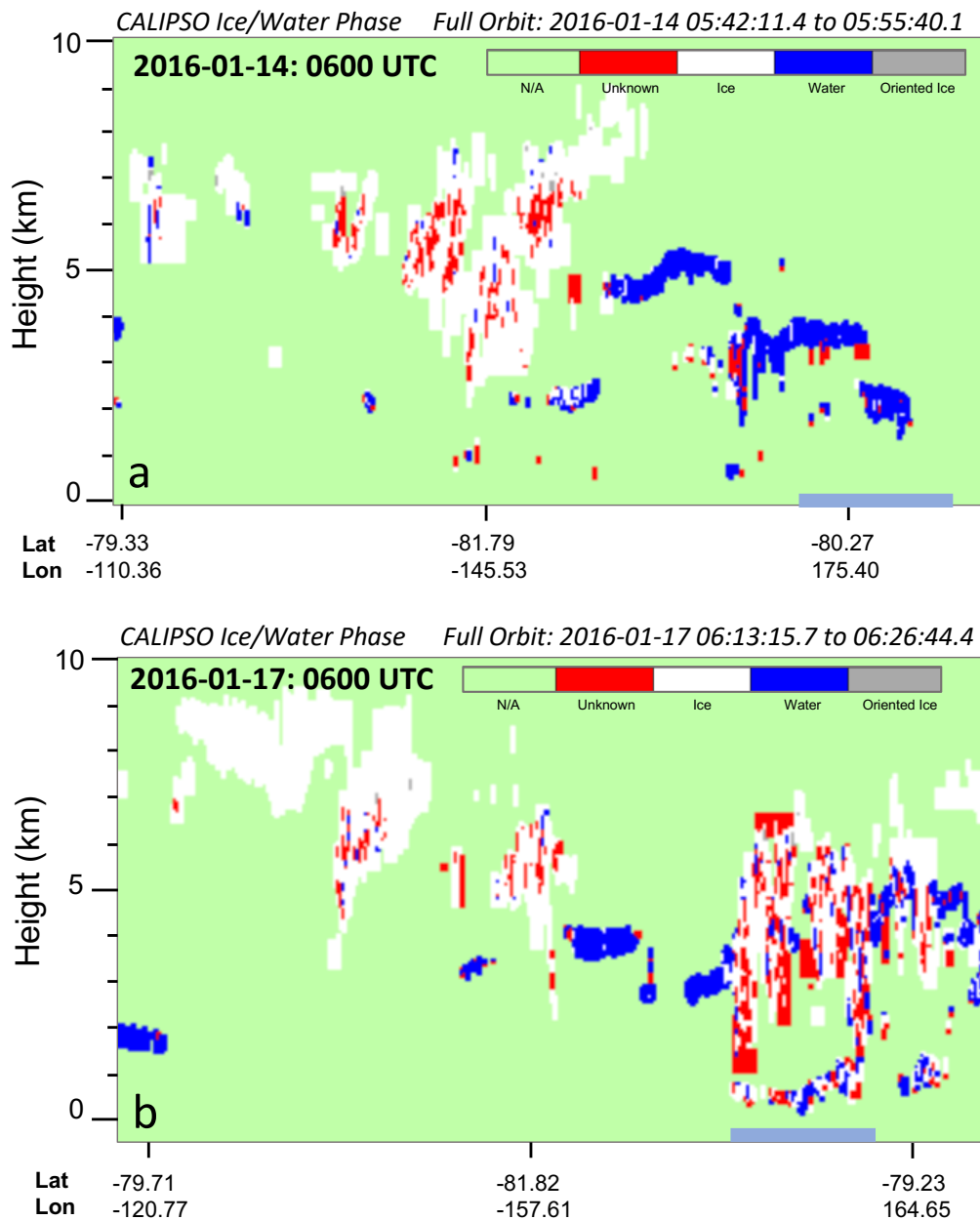
Figure 10. Observed vertical profile of cloud phase from the CALIPSO satellite over the RIS at around 06 UTC on a) the 14th of January and b) the 17th of January. The blue bars at the bottom of each panel highlight the part of each satellite ground track that is over the western region of the RIS highlighted in Fig. 1. Note that 06 UTC is equivalent to 18 LT over the Ross Ice Shelf.
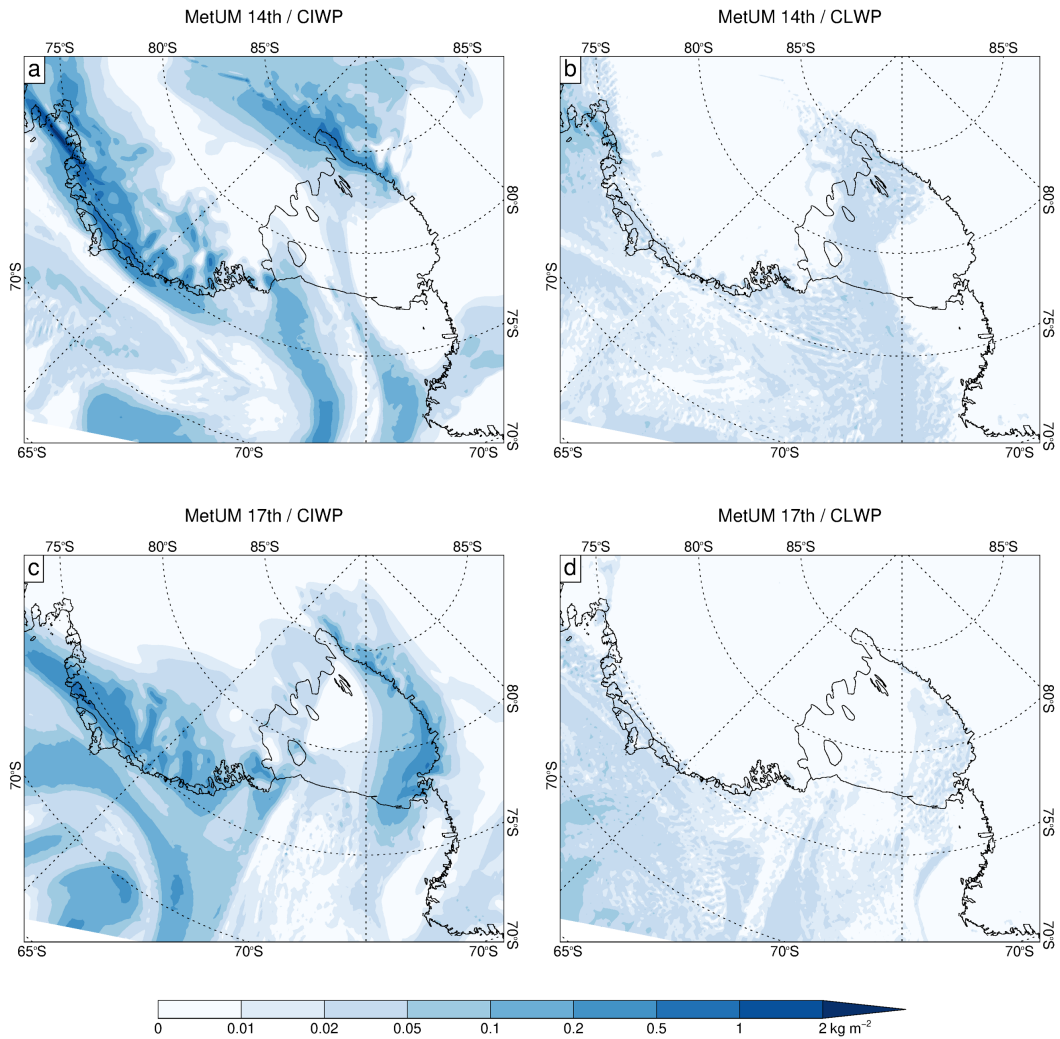
Figure 11. Maps of West Antarctica showing the cloud ice water path (CIWP; left column; a, c; kg m^{-2}) and cloud liquid water path (CLWP; right column; b, d; kg m^{-2}) at 12 UTC on the 14th of January 2016 (top row; a, b) and 12 UTC on the 17th of January 2016 (bottom row; c, d) from the MetUM, based on instantaneous values. Note that equivalent cloud ice/liquid water path information from the HIRHAM5 simulation was not available. Note also that 12 UTC is equivalent to 00 LT over the Ross Ice Shelf.
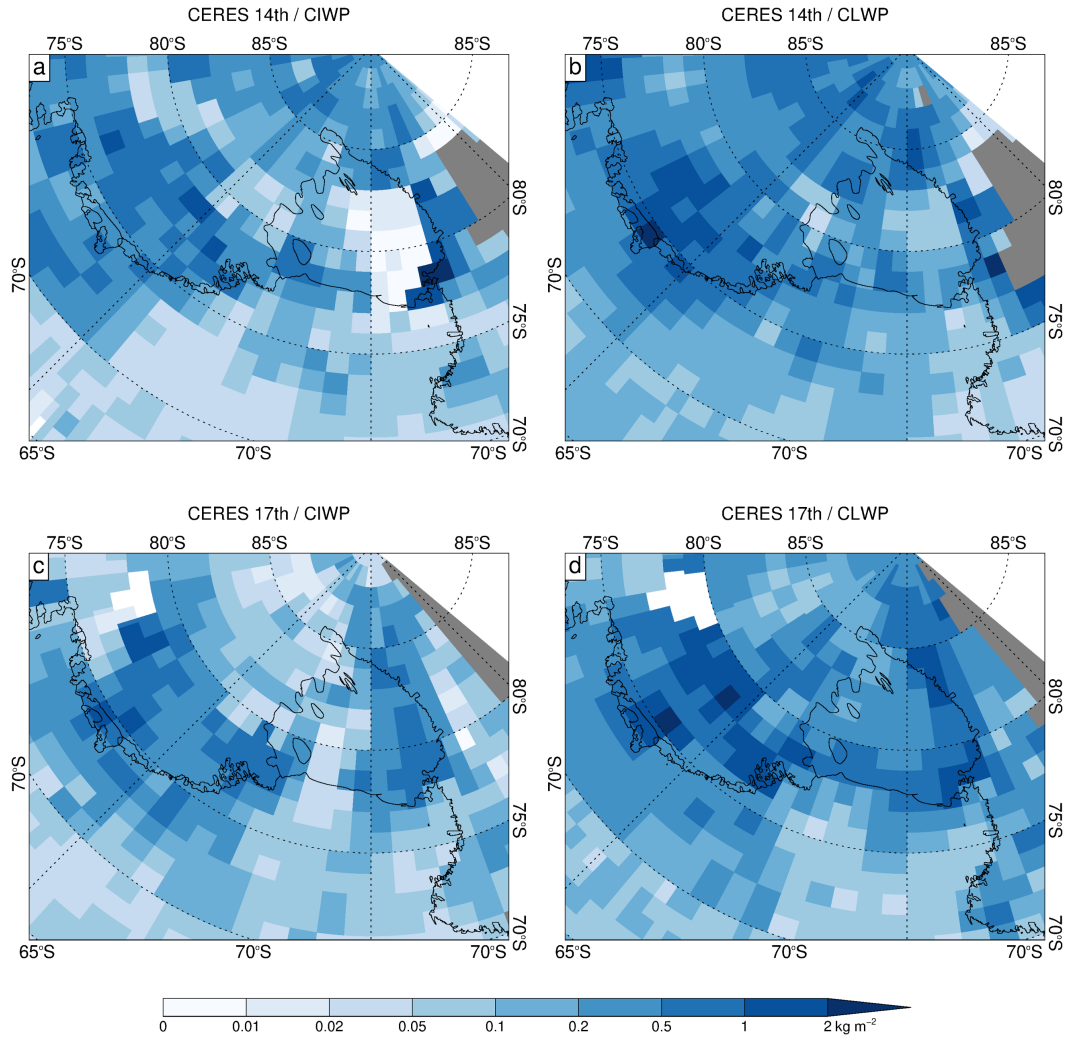
Figure 12. Maps of West Antarctica showing the cloud ice water path (CIWP; left column; a, c; kg m^{-2}) and cloud liquid water path (CLWP; right column; b, d; kg m^{-2}) at 12 UTC on the 14th of January 2016 (top row; a, b) and 12 UTC on the 17th of January 2016 (bottom row; c, d) from CERES observations, based on 3-hourly averages. Note that 12 UTC is equivalent to 00 LT over the Ross Ice Shelf.

6   Discussion

The distinct melt-free region that is observed over the western sector of the RIS from the 16th to the 18th of January (Fig. 3) coincides with observations from MODIS showing cloudy conditions (Fig. 9). Observations from CALIPSO and CERES show that these cloud conditions are characterised by both liquid-water and ice-water clouds (Figs. 10 and 12). However, the firn models erroneously simulate sustained melting over this region/period, which is attributed to HIRHAM5 and MetUM simulat-

ing an excessive increase in nighttime downwelling LW flux from around 180-200 W m^{-2} to 280 W m^{-2} over the course of a few days (Fig. 5), leading to an excessive amount of energy at the surface available for melt. Moreover, although both HIRHAM5 and MetUM capture the cloudy conditions over the western sector of the RIS on the 17th, they likely both have deficiencies in the representation of cloud phase (Fig. 11). In particular, for this event the MetUM simulates much higher amounts of cloud ice-water over the western sector of the RIS compared to cloud liquid-water (Fig. 11), which is in disagreement with both CALIPSO and CERES observations that suggest that both phases are important (Figs. 10 and 12).

Discrepancies in cloud liquid and ice water paths between the satellites and models may arise from uncertainties associated with the observations. For example, two downsides of CERES are its low resolution and that occasionally cloud properties are missing - this is dealt with by interpolating from the nearest timesteps (CERES, 2021). In addition, uncertainties in CALIPSO's cloud phase identification can arise from multiple scattering by water clouds, which exhibit significant depolarisation, and horizontally oriented ice particles that are nearly non-depolarising (Hu et al., 2009). Therefore, CALIPSO may introduce uncertainties to the vertical profile of cloud phases, including the presence of "ice/unknown" phases above the surface melting area over the RIS (Fig. 10b). Similarly, mixed-phase clouds, like those indicated by the CALIPSO measurements for 16th to the 18th, are notoriously difficult to simulate accurately in climate models (Bodas-Salcedo et al., 2012; Furtado et al., 2016). However, the discrepancies between the CERES and MetUM estimates of cloud-liquid water path on the 17th of January are extremely large (two orders of magnitude), which suggests that the more likely reason for this is that the MetUM actually severely underestimates cloud-liquid water and not due to uncertainties with the observations.

However, if the larger amounts of cloud liquid water that are observed by CALIPSO and CERES on the 17th had been simulated by HIRHAM5 and MetUM, then the models would likely be associated with even larger downwelling surface LW fluxes (Zhang et al., 1996). If this was the case then the additional surface melting that would be associated with this would be inconsistent with the passive microwave measurements showing that the western portion of the RIS was melt-free during this time. This therefore suggests that other factors, in addition to ice-to-liquid partitioning of cloud water, could be poorly represented by the models and result in an overestimation of nighttime net surface radiative flux. For example, the underlying problems with simulated cloud microphysics may be causing this by affecting other micro and macrophysical properties of the clouds that we have not been able to assess here, such as cloud temperature and altitude, and cloud microphysical properties like the size of water droplets or ice crystals. Unfortunately, there are neither the AWS radiation measurements, satellite cloud products, nor vertically resolved model output fields available to explicitly assess these errors.

Addressing such deficiencies in cloud schemes will require increasing the number of well-instrumented Antarctic stations that are able to make comprehensive measurements of radiation and clouds (Lubin et al., 2020; Zhang et al., 2023). Efforts are underway to improve the surface observing network to have full four-component radiation measurements, which will also require additional care to ensure the measurements are of sufficient quality to be used in future studies. Repeating a study such as this for a melt event that includes such measurements would be worthwhile, as would repeating the MetUM simulations using its recently developed double-moment microphysics scheme to examine whether this increased the fidelity of cloud microphysical properties in this case study (Field et al., 2023). Additionally, more information on the phase of clouds in Antarctica and their vertical structure using flight campaigns are also required. Novel attempts to measure the amount of cloud

liquid-water and ice-water using radiosondes have recently been developed and are suitable for use in Antarctica (Smith et al., 2019).

Previous studies have already shown that the MetUM has deficiencies in its representation of complex mixed-phase clouds,
330 particularly related to it simulating Antarctic clouds that contain too much ice-water content and not enough liquid-water content (Gilbert et al., 2020). Other regional atmospheric models also struggle with correctly simulating cloud microphysical processes in such complex regimes (Bodas-Salcedo et al., 2012; Abel et al., 2017; Hyder et al., 2018). Moreover, the representation of cloud properties in general is a long-standing problem in both regional and global atmospheric models despite work to improve parameterisations (Van Wessem et al., 2014, 2018; Lenaerts et al., 2017c; Hines et al., 2019). For example,
335 the parameterisation of sub-grid scale cloud processes and cloud phase partitioning is improved by using higher resolution, but significant biases remain in global and regional models that contribute to SEB biases, particularly over the Southern Ocean (Bodas-Salcedo et al., 2014; Schuddeboom and McDonald, 2021) but also over ice shelves (King et al., 2015; Gilbert et al., 2020). Additionally, Gilbert et al. (2020) highlighted the need to improve phase partitioning throughout the vertical profile, as poor representation of cloud layers can also create biases considerable enough to affect surface melting.
340 The impact of cloud properties on melt has also been studied in Greenland and over Arctic sea ice, where similar biases in atmospheric models have been identified (Van Tricht et al., 2016; Lenaerts et al., 2017a, 2020; Huang et al., 2019). Improving cloud parameterisation schemes will therefore likely improve the representation of Arctic as well as Antarctic melt.

7 Conclusions

This study examines the representation of an extensive melt event that occurred over the RIS during January 2016 by the
345 HIRHAM5 and MetUM high-resolution regional atmospheric models, as well as a physically-based, multi-layer, offline coupled firn model forced by both HIRHAM5 and MetUM output. The results show that both the HIRHAM5 and MetUM simulations considerably underestimated the number of melt days that occurred during the event, which is likely due to both limitations in their own ice/snow surface schemes and an absence of spin-up. However, using HIRHAM5 and MetUM output to force the offline coupled firn model resulted in a considerable improvement in modelled melt. Although the firn model repre-
350 sents the firn layer in a sophisticated manner, including processes such as meltwater percolation, retention, and refreezing, the considerable improvement in the simulation of the melt event by this model is also likely due to it being adequately spun up to ensure a realistic representation of snow and firn properties. However, despite its sophistication, the offline coupled firn model was unable to realistically represent the complete melt pattern over the RIS, and in particular the distinct melt-free region that occurs over the western sector of the RIS from the 16th to the 18th of January.
355 We speculate that the sustained melting over the western sector of the RIS that is wrongly simulated by the firn model originates from the HIRHAM5 and MetUM output used for forcing. In particular, both models erroneously simulate zero/positive values of nighttime/minimum net surface radiation flux (and associated SEB) over the western sector of the RIS during this period, which is broadly consistent with an absence of freezing. This occurs in response to the models simulating a considerable increase in surface downwelling LW flux from around 180 to 200 W m^{-2} to around 280 W m^{-2} over the course of a few

360 days, leading to an excessive amount of energy at the surface available for melt. Our results suggest that deficiencies in cloud properties by HIRHAM5 and MetUM, in addition to ice-to-liquid partitioning of cloud water, are likely to be partly responsible for the misrepresentation of surface downwelling LW flux/surface melting over the western RIS, and not deficiencies in their representation of cloud cover. Other possible factors include the misrepresentation of cloud temperature, cloud altitude, and the size of water droplets or ice crystals.

365 This study emphasises the complexity of the processes governing ice shelf melt, and the need for further detailed in-situ measurements of radiative flux and cloud properties over Antarctic ice shelves to better understand these processes and improve their representation in models. It particularly highlights the urgent need for improvement in the representation of cloud phase partitioning in models.

Data availability. The satellite-based melt data used in this study are available here: https://doi.org/10.5285/ffd24dd7-e201-4a02-923f-
370 038680bf7bb5. The MODIS, CERES, and CALIPSO data are available from NASA (National Aeronautics and Space Administration). The MODIS data are available here: https://modis.gsfc.nasa.gov/data/dataprod/mod06.php. The CERES data are available here: https://ceres-tool.larc.nasa.gov/ord-tool/jsp/SYN1degEd41Selection.jsp. The CALIPSO data are available here: https://eosweb.larc.nasa.gov/clouds). The AWS data are available here for: a) Sabrina https://doi.org/10.48567/y3s5-3864, b) Elaine https://doi.org/10.48567/tytb-dk68, c) Marilyn https://doi.org/10.48567/kxn6-6246, and d) Schwerdtfeger https://doi.org/10.48567/96v9-mz68. The model output from the HIRHAM5, MetUM,
375 and offline coupled firn model simulations are available here: https:\doi.org/10.5281/zenodo.8355571

Author contributions. NH and AO conceived the study. NH, AO, and FB ran the model simulations. NH, AO, XZ, and TP analysed the data. NH, AO, and XZ wrote the initial draft. TB, EG, PL, RM, RP, SW, ML, and SS contributed to analysis of the results and reviewing the writing.

Competing interests. At least one of the (co-)authors is a member of the editorial board of The Cryosphere.

380 *Acknowledgements.* We are grateful for the expert comments by two anonymous referees on an earlier version of this article, which significantly improved it. AO, RM, EG, and RP received support from the European Union's Horizon 2020 research and innovation framework programme under Grant Agreement 101003590 (PolarRES). AO and TB received support from the Natural Environment Research Council (NERC) National Capability International grant SURface FluxEs In AnTarctica (NE/X009319/1). XZ received support from National Science Foundation (NSF) Grant 2229392. PL gratefully acknowledges the financial contributions of Aarhus University Interdisci-
385 plinary Centre for Climate Change (iClimate, Aarhus University). ML received support from the US National Science Foundation Grants 1924730 and 1951603. Additional work by NH and RM is supported by the Danish State through the National Centre for Climate Research (NCKF), furthermore, NH and RM are supported by the Novo Nordisk Foundation project PRECISE (NNF23OC0081251).

References

Abel, S. J., Boutle, I. A., Waite, K., Fox, S., Brown, P. R., Cotton, R., Lloyd, G., Choularton, T. W., and Bower, K. N.: The role of precipitation in controlling the transition from stratocumulus to cumulus clouds in a Northern Hemisphere cold-air outbreak, Journal of the Atmospheric Sciences, 74, 2293–2314, https://doi.org/10.1175/JAS-D-16-0362.1, 2017.

Barrett, A. I., Hogan, R. J., and Forbes, R. M.: Why are mixed-phase altocumulus clouds poorly predicted by large-scale models? Part 1. Physical processes, Journal of Geophysical Research: Atmospheres, 122, 9903–9926, https://doi.org/10.1002/2016JD026321, 2017.

Best, M. J., Pryor, M., Clark, D., Rooney, G. G., Essery, R., Ménard, C., Edwards, J., Hendry, M., Porson, A., Gedney, N., et al.: The Joint UK Land Environment Simulator (JULES), model description–Part 1: energy and water fluxes, Geoscientific Model Development, 4, 677–699, https://doi.org/10.5194/gmd-4-677-2011, 2011.

Boberg, F., Mottram, R., Hansen, N., Yang, S., and Langen, P. L.: Uncertainties in projected surface mass balance over the polar ice sheets from dynamically downscaled EC-Earth models, The Cryosphere, 16, 17–33, https://doi.org/10.5194/tc-16-17-2022, 2022.

Bodas-Salcedo, A., Williams, K., Field, P., and Lock, A.: The surface downwelling solar radiation surplus over the Southern Ocean in the Met Office model: The role of midlatitude cyclone clouds, Journal of Climate, 25, 7467–7486, https://doi.org/10.1175/JCLI-D-11-00702.1, 2012.

Bodas-Salcedo, A., Williams, K. D., Ringer, M. A., Beau, I., Cole, J. N., Dufresne, J.-L., Koshiro, T., Stevens, B., Wang, Z., and Yokohata, T.: Origins of the solar radiation biases over the Southern Ocean in CFMIP2 models, Journal of Climate, 27, 41–56, https://doi.org/10.1175/JCLI-D-13-00169.1, 2014.

Bozkurt, D., Rondanelli, R., Marín, J. C., and Garreaud, R.: Foehn event triggered by an atmospheric river underlies record-setting temperature along continental Antarctica, Journal of Geophysical Research: Atmospheres, 123, 3871–3892, https://doi.org/10.1002/2017JD027796, 2018.

Carter, J., Leeson, A., Orr, A., Kittel, C., and van Wessem, J. M.: Variability in Antarctic surface climatology across regional climate models and reanalysis datasets, The Cryosphere, 16, 3815–3841, https://doi.org/10.5194/tc-16-3815-2022, 2022.

CERES, N.: CERES and GEO-Enhanced TOA, Within-Atmosphere and Surface Fluxes, Clouds and Aerosols 3-Hourly Terra-Aqua Edition4A, https://doi.org/10.5067/TERRA+AQUA/CERES/SYN1DEG-3HOUR_L3.004A, 2017.

CERES, N.: CERES_SYN1deg_Ed4A Data Quality Summary (4/8/2021), https://ceres.larc.nasa.gov/documents/DQ_summaries/CERES_SYN1deg_Ed4A_DQS.pdf, 2021.

Christensen, O. B., Drews, M., Christensen, J. H., Dethloff, K., Ketelsen, K., Hebestadt, I., and Rinke, A.: The HIRHAM regional climate model. Version 5 (beta), 2007.

Coggins, J. H., McDonald, A. J., and Jolly, B.: Synoptic climatology of the Ross Ice Shelf and Ross Sea region of Antarctica: k-means clustering and validation, International journal of climatology, 34, 2330–2348, https://doi.org/10.1002/joc.3842, 2014.

de Roda Husman, S., Lhermitte, S., Bolibar, J., Izeboud, M., Hu, Z., Shukla, S., van der Meer, M., Long, D., and Wouters, B.: A high-resolution record of surface melt on Antarctic ice shelves using multi-source remote sensing data and deep learning, Remote Sensing of Environment, 301, 113 950, https://doi.org/10.1016/j.rse.2023.113950, 2024.

Deb, P., Orr, A., Bromwich, D. H., Nicolas, J. P., Turner, J., and Hosking, J. S.: Summer drivers of atmospheric variability affecting ice shelf thinning in the Amundsen Sea Embayment, West Antarctica, Geophysical Research Letters, 45, 4124–4133, https://doi.org/10.1029/2018GL077092, 2018.

Dee, D. P., Uppala, S. M., Simmons, A. J., Berrisford, P., Poli, P., Kobayashi, S., Andrae, U., Balmaseda, M., Balsamo, G., Bauer, d. P., et al.: The ERA-Interim reanalysis: Configuration and performance of the data assimilation system, Quarterly Journal of the royal meteorological society, 137, 553–597, https://doi.org/https://doi.org/10.1002/qj.828, 2011.

Donat-Magnin, M., Jourdain, N. C., Gallée, H., Amory, C., Kittel, C., Fettweis, X., Wille, J. D., Favier, V., Drira, A., and Agosta, C.: Interannual variability of summer surface mass balance and surface melting in the Amundsen sector, West Antarctica, The Cryosphere, 14, 229–249, https://doi.org/10.5194/tc-14-229-2020, 2020.

Dupont, T. and Alley, R.: Assessment of the importance of ice-shelf buttressing to ice-sheet flow, Geophysical Research Letters, 32, https://doi.org/10.1029/2004GL022024, 2005.

Feron, S., Cordero, R. R., Damiani, A., Malhotra, A., Seckmeyer, G., and Llanillo, P.: Warming events projected to become more frequent and last longer across Antarctica, Scientific Reports, 11, 19 564, https://doi.org/10.1038/s41598-021-98619-z, 2021.

Field, P. R., Hill, A., Shipway, B., Furtado, K., Wilkinson, J., Miltenberger, A., Gordon, H., Grosvenor, D. P., Stevens, R., and Van Weverberg, K.: Implementation of a double moment cloud microphysics scheme in the UK met office regional numerical weather prediction model, Quarterly Journal of the Royal Meteorological Society, https://doi.org/10.1002/qj.4414, 2023.

Firn Symposium team, T.: Firn on ice sheets, Nature Reviews Earth & Environment, pp. 1–21, https://doi.org/10.1038/s43017-023-00507-9, 2024.

Fox-Kemper, B., Hewitt, H., C. Xiao, G. A., S.S. Drijfhout, T. E., Golledge, N., M. Hemer, R. K., Krinner, G., Mix, A., Notz, D., Nowicki, S., Nurhati, I., Ruiz, L., Sallée, J.-B., Slangen, A., and Yu, Y.: Ocean, Cryosphere and Sea Level Change. In Climate Change 2021: The Physical Science Basis. Contribution of Working Group I to the Sixth Assessment Report of the Intergovernmental Panel on Climate Change, pp. 1211–1362, https://doi.org/10.1017/9781009157896.011, 2021.

Furtado, K., Field, P., Boutle, I., Morcrette, C., and Wilkinson, J.: A physically based subgrid parameterization for the production and maintenance of mixed-phase clouds in a general circulation model, Journal of the Atmospheric Sciences, 73, 279–291, https://doi.org/10.1175/JAS-D-15-0021.1, 2016.

Gilbert, E. and Kittel, C.: Surface melt and runoff on Antarctic ice shelves at 1.5 C, 2 C, and 4 C of future warming, Geophysical Research Letters, 48, e2020GL091 733, https://doi.org/10.1029/2020GL091733, 2021.

Gilbert, E., Orr, A., King, J. C., Renfrew, I., Lachlan-Cope, T., Field, P., and Boutle, I.: Summertime cloud phase strongly influences surface melting on the Larsen C ice shelf, Antarctica, Quarterly Journal of the Royal Meteorological Society, 146, 1575–1589, https://doi.org/10.1002/qj.3753, 2020.

Gilbert, E., Orr, A., Renfrew, I. A., King, J. C., and Lachlan-Cope, T.: A 20-Year Study of Melt Processes Over Larsen C Ice Shelf Using a High-Resolution Regional Atmospheric Model: 2. Drivers of Surface Melting, Journal of Geophysical Research: Atmospheres, 127, e2021JD036 012, https://doi.org/10.1002/essoar.10508261.1, 2022.

Hansen, N., Langen, P. L., Boberg, F., Forsberg, R., Simonsen, S. B., Thejll, P., Vandecrux, B., and Mottram, R.: Downscaled surface mass balance in Antarctica: impacts of subsurface processes and large-scale atmospheric circulation, The Cryosphere, 15, 4315–4333, https://doi.org/10.5194/tc-15-4315-2021, 2021.

Heinemann, G., Glaw, L., and Willmes, S.: A satellite-based climatology of wind-induced surface temperature anomalies for the Antarctic, Remote Sensing, 11, 1539, https://doi.org/10.3390/rs11131539, 2019.

Hines, K. M., Bromwich, D. H., Wang, S.-H., Silber, I., Verlinde, J., and Lubin, D.: Microphysics of summer clouds in central West Antarctica simulated by the Polar Weather Research and Forecasting model (WRF) and the Antarctic Mesoscale Prediction System (AMPS), Atmospheric Chemistry and Physics, 19, 12 431–12 454, https://doi.org/10.5194/acp-19-12431-2019, 2019.

Hinkelman, L. M. and Marchand, R.: Evaluation of CERES and CloudSat Surface Radiative Fluxes Over Macquarie Island, the Southern Ocean, Earth Space and Science, 7, e2020EA001 224, https://doi.org/10.1029/2020EA001224, 2020.

Hu, Y., Winker, D., Vaughan, M., Lin, B., Omar, A., Trepte, C., Flittner, D., Yang, P., Nasiri, S. L., Baum, B., et al.: CALIPSO/CALIOP cloud phase discrimination algorithm, Journal of Atmospheric and Oceanic Technology, 26, 2293–2309, https://doi.org/10.1175/2009JTECHA1280.1, 2009.

Huang, Y., Dong, X., Bailey, D. A., Holland, M. M., Xi, B., DuVivier, A. K., Kay, J. E., Landrum, L. L., and Deng, Y.: Thicker clouds and accelerated Arctic sea ice decline: The atmosphere-sea ice interactions in spring, Geophysical Research Letters, 46, 6980–6989, https://doi.org/10.1029/2019GL082791, 2019.

Hyder, P., Edwards, J. M., Allan, R. P., Hewitt, H. T., Bracegirdle, T. J., Gregory, J. M., Wood, R. A., Meijers, A. J., Mulcahy, J., Field, P., et al.: Critical Southern Ocean climate model biases traced to atmospheric model cloud errors, Nature communications, 9, 3625, https://doi.org/10.1038/s41467-018-05634-2, 2018.

Inoue, J., Sato, K., Rinke, A., Cassano, J. J., Fettweis, X., Heinemann, G., Matthes, H., Orr, A., Phillips, T., Seefeldt, M., et al.: Clouds and radiation processes in regional climate models evaluated using observations over the ice-free Arctic Ocean, Journal of Geophysical Research: Atmospheres, 126, e2020JD033 904, https://doi.org/10.1029/2020JD033904, 2021.

Jakobs, C. L., Reijmer, C. H., van den Broeke, M. R., Van de Berg, W., and Van Wessem, J.: Spatial Variability of the Snowmelt-Albedo Feedback in Antarctica, Journal of Geophysical Research: Earth Surface, 126, e2020JF005 696, https://doi.org/10.1029/2020JF005696, 2021.

Johnson, A., Fahnestock, M., and Hock, R.: Evaluation of passive microwave melt detection methods on Antarctic Peninsula ice shelves using time series of Sentinel-1 SAR, Remote Sensing of Environment, 250, 112 044, https://doi.org/10.1016/j.rse.2020.112044, 2020.

Johnson, A., Hock, R., and Fahnestock, M.: Spatial variability and regional trends of Antarctic ice shelf surface melt duration over 1979–2020 derived from passive microwave data, Journal of Glaciology, 68, 533–546, https://doi.org/10.1017/jog.2021.112, 2022.

Keenan, E., Wever, N., Dattler, M., Lenaerts, J., Medley, B., Kuipers Munneke, P., and Reijmer, C.: Physics-based SNOWPACK model improves representation of near-surface Antarctic snow and firn density, The Cryosphere, 15, 1065–1085, https://doi.org/10.5194/tc-15-1065-2021, 2021.

Kim, S., Park, S., and Shin, J.: Impact of subgrid variation of water vapor on longwave radiation in a general circulation model, Journal of Advances in Modeling Earth Systems, 12, e2019MS001 926, https://doi.org/10.1029/2019MS001926, 2020.

King, J., Gadian, A., Kirchgaessner, A., Kuipers Munneke, P., Lachlan-Cope, T., Orr, A., Reijmer, C., Van Den Broeke, M., Van Wessem, J., and Weeks, M.: Validation of the summertime surface energy budget of Larsen C Ice Shelf (Antarctica) as represented in three high-resolution atmospheric models, Journal of Geophysical Research: Atmospheres, 120, 1335–1347, https://doi.org/10.1002/2014JD022604, 2015.

Kingslake, J., Ely, J. C., Das, I., and Bell, R. E.: Widespread movement of meltwater onto and across Antarctic ice shelves, Nature, 544, 349–352, https://doi.org/10.1038/nature22049, 2017.

Kittel, C., Amory, C., Agosta, C., Jourdain, N. C., Hofer, S., Delhasse, A., Doutreloup, S., Huot, P.-V., Lang, C., Fichefet, T., et al.: Diverging future surface mass balance between the Antarctic ice shelves and grounded ice sheet, The Cryosphere, 15, 1215–1236, https://doi.org/10.5194/tc-15-1215-2021, 2021.

Kretzschmar, J., Stapf, J., Klocke, D., Wendisch, M., and Quaas, J.: Employing airborne radiation and cloud microphysics observations to improve cloud representation in ICON at kilometer-scale resolution in the Arctic, Atmospheric Chemistry and Physics, 20, 13 145–13 165, https://doi.org/10.5194/acp-20-13145-2020, 2020.

500 Kuipers Munneke, P., Ligtenberg, S. R., Van Den Broeke, M. R., and Vaughan, D. G.: Firn air depletion as a precursor of Antarctic ice-shelf collapse, Journal of Glaciology, 60, 205–214, https://doi.org/10.3189/2014JoG13J183, 2014.

Langen, P., Mottram, R., Christensen, J., Boberg, F., Rodehacke, C., Stendel, M., Van As, D., Ahlstrøm, A., Mortensen, J., Rysgaard, S., et al.: Quantifying energy and mass fluxes controlling Godthåbsfjord freshwater input in a 5-km simulation (1991–2012), Journal of Climate, 28, 3694–3713, https://doi.org/10.1175/JCLI-D-14-00271.1, 2015.

505 Langen, P. L., Fausto, R. S., Vandecrux, B., Mottram, R. H., and Box, J. E.: Liquid water flow and retention on the Greenland ice sheet in the regional climate model HIRHAM5: Local and large-scale impacts, Frontiers in Earth Science, 4, 110, https://doi.org/10.3389/feart.2016.00110, 2017.

Lawson, R. P. and Gettelman, A.: Impact of Antarctic mixed-phase clouds on climate, Proceedings of the National Academy of Sciences, 111, 18 156–18 161, https://doi.org/10.1073/pnas.1418197111, 2014.

510 Lazzara, M. A., Weidner, G. A., Keller, L. M., Thom, J. E., and Cassano, J. J.: Antarctic automatic weather station program: 30 years of polar observation, Bulletin of the American Meteorological Society, 93, 1519–1537, https://doi.org/10.1175/BAMS-D-11-00015.1, 2012.

Lenaerts, J., Lhermitte, S., Drews, R., Ligtenberg, S., Berger, S., Helm, V., Smeets, C., Broeke, M. v. d., Van De Berg, W. J., Van Meijgaard, E., et al.: Meltwater produced by wind–albedo interaction stored in an East Antarctic ice shelf, Nature climate change, 7, 58–62, https://doi.org/10.1038/nclimate3180, 2017a.

515 Lenaerts, J. T., Ligtenberg, S. R., Medley, B., Van de Berg, W. J., Konrad, H., Nicolas, J. P., Van Wessem, J. M., Trusel, L. D., Mulvaney, R., Tuckwell, R. J., Hogg, A. E., and Thomas, E. R.: Climate and surface mass balance of coastal West Antarctica resolved by regional climate modelling, Annals of Glaciology, 59, 29–41, https://doi.org/10.1017/aog.2017.42, 2017b.

Lenaerts, J. T., Van Tricht, K., Lhermitte, S., and L'Ecuyer, T. S.: Polar clouds and radiation in satellite observations, reanalyses, and climate models, Geophysical Research Letters, 44, 3355–3364, https://doi.org/10.1002/2016GL072242, 2017c.

520 Lenaerts, J. T., Gettelman, A., Van Tricht, K., van Kampenhout, L., and Miller, N. B.: Impact of cloud physics on the Greenland ice sheet Near-Surface climate: A study with the Community Atmosphere Model, Journal of Geophysical Research: Atmospheres, 125, e2019JD031 470, https://doi.org/10.1029/2019JD031470, 2020.

Li, W., Wu, Y., and Hu, X.: The Processes-Based Attributes of Four Major Surface Melting Events over the Antarctic Ross Ice Shelf, Advances in Atmospheric Sciences, pp. 1–9, https://doi.org/10.1007/s00376-023-2287-3, 2023.

525 Lo, J. C.-F., Yang, Z.-L., and Pielke Sr, R. A.: Assessment of three dynamical climate downscaling methods using the Weather Research and Forecasting (WRF) model, Journal of Geophysical Research: Atmospheres, 113, https://doi.org/10.1029/2007JD009216, 2008.

Loeb, N., Su, W., Doelling, D., Wong, T., Minnis, P., Thomas, S., and Miller, W.: 5.03 - Earth's Top-of-Atmosphere Radiation Budget, in: Comprehensive Remote Sensing, edited by Liang, S., pp. 67–84, Elsevier, Oxford, https://doi.org/10.1016/B978-0-12-409548-9.10367-7, 2018.

530 Lubin, D., Zhang, D., Silber, I., Scott, R. C., Kalogeras, P., Battaglia, A., Bromwich, D. H., Cadeddu, M., Eloranta, E., Fridlind, A., et al.: AWARE: The atmospheric radiation measurement (ARM) west Antarctic radiation experiment, Bulletin of the American Meteorological Society, 101, E1069–E1091, https://doi.org/10.1175/BAMS-D-18-0278.1, 2020.

McCusker, G. Y., Vüllers, J., Achtert, P., Field, P., Day, J. J., Forbes, R., Price, R., O'Connor, E., Tjernström, M., Prytherch, J., et al.: Evaluating Arctic clouds modelled with the Unified Model and Integrated Forecasting System, Atmospheric Chemistry and Physics, 23,
535 4819–4847, https://doi.org/10.5194/acp-23-4819-2023, 2023.

Mottram, R., Boberg, F., Langen, P., Yang, S., Rodehacke, C., Christensen, J. H., and Madsen, M. S.: Surface mass balance of the Greenland ice sheet in the regional climate model HIRHAM5: Present state and future prospects, Low Temperature Science, 75, 105–115, https://doi.org/10.14943/lowtemsci.75.105, 2017.

Mousavi, M., Colliander, A., Miller, J. Z., and Kimball, J. S.: A novel approach to map the intensity of surface melting on the Antarctica ice sheet using SMAP L-band microwave radiometry, IEEE Journal of Selected Topics in Applied Earth Observations and Remote Sensing, 15, 1724–1743, https://doi.org/10.1109/JSTARS.2022.3147430, 2022.

Nicolas, J. P. and Bromwich, D. H.: Climate of West Antarctica and influence of marine air intrusions, Journal of Climate, 24, 49–67, https://doi.org/10.1175/2010JCLI3522.1, 2011.

Nicolas, J. P., Vogelmann, A. M., Scott, R. C., Wilson, A. B., Cadeddu, M. P., Bromwich, D. H., Verlinde, J., Lubin, D., Russell, L. M., Jenkinson, C., et al.: January 2016 extensive summer melt in West Antarctica favoured by strong El Niño, Nature communications, 8, 15 799, https://doi.org/10.1038/ncomms15799, 2017.

Orr, A., Cresswell, D., Marshall, G. J., Hunt, J. C., Sommeria, J., Wang, C.-G., and Light, M.: A 'low-level' explanation for the recent large warming trend over the western Antarctic Peninsula involving blocked winds and changes in zonal circulation, Geophysical Research Letters, 31, https://doi.org/10.1029/2003GL019160, 2004.

Orr, A., Hunt, J. C., Capon, R., Sommeria, J., Cresswell, D., and Owinoh, A.: Coriolis effects on wind jets and cloudiness along coasts, Weather, 60, 291–299, https://doi.org/10.1256/wea.219.04, 2005.

Orr, A., Phillips, T., Webster, S., Elvidge, A., Weeks, M., Hosking, S., and Turner, J.: Met Office Unified Model high-resolution simulations of a strong wind event in Antarctica, Quarterly Journal of the Royal Meteorological Society, 140, 2287–2297, https://doi.org/10.1002/qj.2296, 2014.

Orr, A., Deb, P., Clem, K. R., Gilbert, E., Bromwich, D. H., Boberg, F., Colwell, S., Hansen, N., Lazzara, M. A., Mooney, P. A., et al.: Characteristics of surface "melt potential" over Antarctic ice shelves based on regional atmospheric model simulations of summer air temperature extremes from 1979/80 to 2018/19, Journal of Climate, pp. 1–61, https://doi.org/10.1175/JCLI-D-22-0386.1, 2023.

Otosaka, I. N., Shepherd, A., Ivins, E. R., Schlegel, N.-J., Amory, C., van den Broeke, M., Horwath, M., Joughin, I., King, M., Krinner, G., Nowicki, S., Payne, T., Rignot, E., Scambos, T., Simon, K. M., Smith, B., Sandberg Sørensen, L., Velicogna, I., Whitehouse, P., A, G., Agosta, C., Ahlstrøm, A. P., Blazquez, A., Colgan, W., Engdahl, M., Fettweis, X., Forsberg, R., Gallée, H., Gardner, A., Gilbert, L., Gourmelen, N., Groh, A., Gunter, B. C., Harig, C., Helm, V., Khan, S. A., Konrad, H., Langen, P., Lecavalier, B., Liang, C.-C., Loomis, B., McMillan, M., Melini, D., Mernild, S. H., Mottram, R., Mouginot, J., Nilsson, J., Noël, B., Pattle, M. E., Peltier, W. R., Pie, N., Sasgen, I., Save, H., Seo, K.-W., Scheuchl, B., Schrama, E., Schröder, L., Simonsen, S. B., Slater, T., Spada, G., Sutterley, T., Vishwakarma, B. D., van Wessem, J. M., Wiese, D., van der Wal, W., and Wouters, B.: Mass balance of the Greenland and Antarctic ice sheets from 1992 to 2020, Earth System Science Data, 15, 1597–1616, https://doi.org/10.5194/essd-15-1597-2023, 2023.

Owinoh, A. Z., Hunt, J. C., Orr, A., Clark, P., Klein, R., Fernando, H., and Nieuwstadt, F. T.: Effects of changing surface heat flux on atmospheric boundary-layer flow over flat terrain, Boundary-layer meteorology, 116, 331–361, https://doi.org/10.1007/s10546-004-2819-z, 2005.

Picard, G., Fily, M., and Gallée, H.: Surface melting derived from microwave radiometers: a climatic indicator in Antarctica, Annals of Glaciology, 46, 29–34, https://doi.org/10.3189/172756407782871684, 2007.

Platnick, S., Ackerman, S., King, M., et al.: MODIS Atmosphere L2 Cloud Product (06_L2). NASA MODIS Adaptive Processing System, Goddard Space Flight Center, USA, https://doi.org/10.5067/MODIS/MOD06_L2.006, 2015.

Pritchard, H., Ligtenberg, S. R., Fricker, H. A., Vaughan, D. G., van den Broeke, M. R., and Padman, L.: Antarctic ice-sheet loss driven by basal melting of ice shelves, Nature, 484, 502–505, https://doi.org/10.1038/nature10968, 2012.

575 Scambos, T., Fricker, H. A., Liu, C.-C., Bohlander, J., Fastook, J., Sargent, A., Massom, R., and Wu, A.-M.: Ice shelf disintegration by plate bending and hydro-fracture: Satellite observations and model results of the 2008 Wilkins ice shelf break-ups, Earth and Planetary Science Letters, 280, 51–60, https://doi.org/10.1016/j.epsl.2008.12.027, 2009.

Scambos, T. A., Hulbe, C., Fahnestock, M., and Bohlander, J.: The link between climate warming and break-up of ice shelves in the Antarctic Peninsula, Journal of Glaciology, 46, 516–530, https://doi.org/10.3189/172756500781833043, 2000.

580 Schuddeboom, A. J. and McDonald, A. J.: The Southern Ocean radiative bias, cloud compensating errors, and equilibrium climate sensitivity in CMIP6 models, Journal of Geophysical Research: Atmospheres, 126, e2021JD035 310, https://doi.org/10.1029/2021JD035310, 2021.

Scott, R. C., Nicolas, J. P., Bromwich, D. H., Norris, J. R., and Lubin, D.: Meteorological drivers and large-scale climate forcing of West Antarctic surface melt, Journal of Climate, 32, 665–684, https://doi.org/10.1175/JCLI-D-18-0233.1, 2019.

Shepherd, A., Ivins, E., Rignot, E., Smith, B., Van Den Broeke, M., Velicogna, I., Whitehouse, P., Briggs, K., Joughin, I., Krinner, G.,
585 Nowicki, S., Payne, T., Scambos, T., Schlegel, N., Geruo, A., Agosta, C., Ahlstrøm, A., Babonis, G., Barletta, V., Blazquez, A., Bonin, J., Csatho, B., Cullather, R., Felikson, D., Fettweis, X., Forsberg, R., Gallee, H., Gardner, A., Gilbert, L., Groh, A., Gunter, B., Hanna, E., Harig, C., Helm, V., Horvath, A., Horwath, M., Khan, S., Kjeldsen, K. K., Konrad, H., Langen, P., Lecavalier, B., Loomis, B., Luthcke, S., McMillan, M., Melini, D., Mernild, S., Mohajerani, Y., Moore, P., Mouginot, J., Moyano, G., Muir, A., Nagler, T., Nield, G., Nilsson, J., Noel, B., Otosaka, I., Pattle, M. E., Peltier, W. R., Pie, N., Rietbroek, R., Rott, H., Sandberg-Sørensen, L., Sasgen, I., Save, H., Scheuchl,
590 B., Schrama, E., Schröder, L., Seo, K. W., Simonsen, S., Slater, T., Spada, G., Sutterley, T., Talpe, M., Tarasov, L., Van De Berg, W. J., Van Der Wal, W., Van Wessem, M., Vishwakarma, B. D., Wiese, D., and Wouters, B.: Mass balance of the Antarctic Ice Sheet from 1992 to 2017, Nature, 558, 219–222, https://doi.org/10.1038/s41586-018-0179-y, 2018.

Smith, H. R., Ulanowski, Z., Kaye, P. H., Hirst, E., Stanley, W., Kaye, R., Wieser, A., Stopford, C., Kezoudi, M., Girdwood, J., et al.: The Universal Cloud and Aerosol Sounding System (UCASS): a low-cost miniature optical particle counter for use in dropsonde or balloon-
595 borne sounding systems, Atmospheric Measurement Techniques, 12, 6579–6599, https://doi.org/10.5194/amt-12-6579-2019, 2019.

Stokes, C. R., Sanderson, J. E., Miles, B. W., Jamieson, S. S., and Leeson, A. A.: Widespread distribution of supraglacial lakes around the margin of the East Antarctic Ice Sheet, Scientific reports, 9, 13 823, https://doi.org/10.1038/s41598-019-50343-5, 2019.

Sundqvist, H.: A parameterization scheme for non-convective condensation including prediction of cloud water content, Quarterly Journal of the Royal Meteorological Society, 104, 677–690, https://doi.org/10.1002/qj.49710444110, 1978.

600 Trusel, L. D., Frey, K. E., Das, S. B., Karnauskas, K. B., Kuipers Munneke, P., Van Meijgaard, E., and Van Den Broeke, M. R.: Divergent trajectories of Antarctic surface melt under two twenty-first-century climate scenarios, Nature Geoscience, 8, 927–932, https://doi.org/10.1038/ngeo2563, 2015.

Tuckett, P. A., Ely, J. C., Sole, A. J., Livingstone, S. J., Davison, B. J., Melchior van Wessem, J., and Howard, J.: Rapid accelerations of Antarctic Peninsula outlet glaciers driven by surface melt, Nature Communications, 10, 4311, https://doi.org/10.1038/s41467-019-12039-
605 2, 2019.

Turner, J., Lu, H., King, J. C., Carpentier, S., Lazzara, M., Phillips, T., and Wille, J.: An Extreme High Temperature Event in Coastal East Antarctica Associated With an Atmospheric River and Record Summer Downslope Winds, Geophysical Research Letters, 49, e2021GL097 108, https://doi.org/10.1029/2021GL097108, 2022.

Van Tricht, K., Lhermitte, S., Lenaerts, J. T., Gorodetskaya, I. V., L'Ecuyer, T. S., Noël, B., van den Broeke, M. R., Turner,
D. D., and van Lipzig, N. M.: Clouds enhance Greenland ice sheet meltwater runoff, Nature communications, 7, 10266,
https://doi.org/10.1038/ncomms10266, 2016.

Van Wessem, J., Reijmer, C., Lenaerts, J., Van de Berg, W., Van den Broeke, M., and Van Meijgaard, E.: Updated cloud physics in
a regional atmospheric climate model improves the modelled surface energy balance of Antarctica, The Cryosphere, 8, 125–135,
https://doi.org/10.5194/tc-8-125-2014, 2014.

Van Wessem, J., van, Berg, W. J. v. d., Noël, B. P., Meijgaard, E. v., Amory, C., Birnbaum, G., Jakobs, C. L., Krüger, K., Lenaerts, J.,
Lhermitte, S., et al.: Modelling the climate and surface mass balance of polar ice sheets using RACMO2–Part 2: Antarctica (1979–2016),
The Cryosphere, 12, 1479–1498, https://doi.org/10.5194/tc-12-1479-2018, 2018.

van Wessem, J. M., van den Broeke, M. R., Wouters, B., and Lhermitte, S.: Variable temperature thresholds of melt pond formation on
Antarctic ice shelves, Nature Climate Change, 13, 161–166, https://doi.org/10.1038/s41558-022-01577-1, 2023.

Van Weverberg, K., Giangrande, S., Zhang, D., Morcrette, C., and Field, P.: On the Role of Macrophysics and Microphysics in Km-Scale
Simulations of Mixed-Phase Clouds during Cold Air Outbreaks, Journal of Geophysical Research: Atmospheres, p. e2022JD037854,
https://doi.org/10.1029/2022JD037854, 2023.

Vignon, É., Alexander, S., DeMott, P., Sotiropoulou, G., Gerber, F., Hill, T., Marchand, R., Nenes, A., and Berne, A.: Challenging and
improving the simulation of mid-level mixed-phase clouds over the high-latitude Southern Ocean, Journal of Geophysical Research:
Atmospheres, 126, e2020JD033490, https://doi.org/10.1029/2020JD033490, 2021.

Walters, D., Boutle, I., Brooks, M., Melvin, T., Stratton, R., Vosper, S., Wells, H., Williams, K., Wood, N., Allen, T., et al.: The Met Office
unified model global atmosphere 6.0/6.1 and JULES global land 6.0/6.1 configurations, Geoscientific Model Development, 10, 1487–
1520, https://doi.org/10.5194/gmd-10-1487-2017, 2017.

Walters, D., Baran, A. J., Boutle, I., Brooks, M., Earnshaw, P., Edwards, J., Furtado, K., Hill, P., Lock, A., Manners, J., et al.: The Met Office
Unified Model global atmosphere 7.0/7.1 and JULES global land 7.0 configurations, Geoscientific Model Development, 12, 1909–1963,
https://doi.org/10.5194/gmd-12-1909-2019, 2019.

Wielicki, B. A., Barkstrom, B. R., Harrison, E. F., Lee III, R. B., Smith, G. L., and Cooper, J. E.: Clouds and the Earth's Radiant
Energy System (CERES): An earth observing system experiment, Bulletin of the American Meteorological Society, 77, 853–868,
https://doi.org/10.1175/1520-0477(1996)077<0853:CATERE>2.0.CO;2, 1996.

Wille, J. D., Favier, V., Dufour, A., Gorodetskaya, I. V., Turner, J., Agosta, C., and Codron, F.: West Antarctic surface melt triggered by
atmospheric rivers, Nature Geoscience, 12, 911–916, https://doi.org/10.1038/s41561-019-0460-1, 2019.

Wille, J. D., Favier, V., Jourdain, N. C., Kittel, C., Turton, J. V., Agosta, C., Gorodetskaya, I. V., Picard, G., Codron, F., Santos, C. L.-D.,
et al.: Intense atmospheric rivers can weaken ice shelf stability at the Antarctic Peninsula, Communications Earth & Environment, 3, 90,
https://doi.org/10.1038/s43247-022-00422-9, 2022.

Wilson, D. R. and Ballard, S. P.: A microphysically based precipitation scheme for the UK Meteorological Office Unified Model, Quarterly
Journal of the Royal Meteorological Society, 125, 1607–1636, https://doi.org/10.1002/qj.49712555707, 1999.

Zhang, M., Xie, S., Liu, X., Zhang, D., Lin, W., Zhang, K., Golaz, J.-C., Zheng, X., and Zhang, Y.: Evaluating EAMv2 Simulated High
Latitude Clouds Using ARM Measurements in the Northern and Southern Hemispheres, Journal of Geophysical Research: Atmospheres,
p. e2022JD038364, https://doi.org/10.1029/2022JD038364, 2023.

Zhang, T., Stamnes, K., and Bowling, S.: Impact of clouds on surface radiative fluxes and snowmelt in the Arctic and subarctic, Journal of
Climate, 9, 2110–2123, https://doi.org/10.1175/1520-0442(1996)009<2110:IOCOSR>2.0.CO;2, 1996.

Zou, X., Bromwich, D. H., Montenegro, A., Wang, S.-H., and Bai, L.: Major surface melting over the Ross Ice Shelf part I: Foehn effect, Quarterly Journal of the Royal Meteorological Society, 147, 2874–2894, https://doi.org/10.1002/qj.4104, 2021.

Zou, X., Rowe, P. M., Gorodetskaya, I., Bromwich, D. H., Lazzara, M. A., Cordero, R. R., Zhang, Z., Kawzenuk, B., Cordeira, J. M., Wille, J. D., et al.: Strong Warming over the Antarctic Peninsula during Combined Atmospheric River and Foehn Events: Contribution of Shortwave Radiation and Turbulence, Journal of Geophysical Research: Atmospheres, p. e2022JD038138, https://doi.org/10.1029/2022JD038138, 2023.